

## **Abstract**

*Title of Thesis:* Advanced FBG Sensor Technique to Measure Effective Chemical Shrinkage and Modulus Evolutions of Polymers with High Polymerization Exothermic Heat

Yejin Kim, Master of Science, 2012

*Thesis Directed by:* Professor Bongtae Han  
Department of Mechanical Engineering

An advanced technique based on a fiber Bragg grating (FBG) sensor is proposed to measure the critical mechanical properties of polymeric materials during polymerization: effective chemical shrinkage and modulus evolutions. Based on the existing technique implemented with convection oven and two different specimen configurations using same size of FBG, challenges associated with implementation are identified and solutions are proposed. Challenges include temperature instability due to high exothermic heat generated during polymerization inside polymer substrate, temperature controllability due to limitations of convection oven, and mechanical

constraint on polymer and fiber during measurement. The proposed system provides modifications to provide easier implementation with accurate results. Modifications such as fabrication of FBG on special fiber, enhancement of heating system, and optimization of system design are combined to provide a tool for rapid but accurate measurement of polymer properties.

The proposed technique significantly improves the ability to characterize the mechanical properties of polymeric materials during polymerization which will enhance the accuracy of predictive modeling for design optimization of a microelectronics product at the conceptual stage of product development.

Advanced FBG Sensor Technique to Measure  
Effective Chemical Shrinkage and Modulus Evolutions of Polymers  
with High Polymerization Exothermic Heat

By

Yejin Kim

Thesis submitted to the Faculty of the Graduate School of the  
University of Maryland, College Park, in partial fulfillment  
of the requirements for the degree of

Master of Science

2012

*Advisory Committee:*

Professor Bongtae Han, Chair/Advisor

Professor Abhijit Dasgupta

Professor Patrick F. McCluskey

**© Copyright by**

**Yejin Kim**

**2012**

## Acknowledgements

Throughout my graduate study, I was blessed to be surrounded by wonderful people who have shown their support and patience, and I am here to express my deepest gratitude to those who have been always there for me.

First of all, I would like to sincerely express my gratitude to my advisor, Dr. Bongtae Han, who made all this possible. I have been very fortunate to have an advisor who provided guidance and advice that lightened up not only my professional life but also my personal life. Throughout the research work during my graduate study, he truly understood my weaknesses and strengths and knew how to train his student with encouragement and patience. His wisdom and knowledge to the highest standards positively inspired and motivated me. I will always be thankful for my advisor who certainly is and will always be one of the greatest impacts on my life.

I would like to thank the members of my thesis committee, Professor Abhijit Dasgupta and Professor Patrick F. McCluskey for their counseling and support in the completion of this thesis.

I would also like to thank my colleagues in LOMSS. I am grateful to Yong Sun who worked with me as a team on this project and everyone else who also have shown support including Bongmin, Kenny, Stephen, Daesuk, Bulong, Mr. Shin, Dr. Oh, and David. I would also like to thank past LOMSS members including Yong Wang and Laura who built foundation of this thesis topic, and Dr. Jang for his helpful advice and support. I was very lucky to work with such wonderful group of people who were always willing to help and cared for one another.

I could not express my gratitude enough to Mr. Thomas Wadford, known as Castle, before he passed away this September. His talent and generosity made it possible for me to successfully conduct my experiments. I enjoyed working with him and want to thank him again for his skillfully machined parts, valuable lessons I have learned from him, and his warm-hearted kindness.

Most importantly, I want to thank my parents and brother who have shown endless support and unconditional love. They were always there for me with patience and love that encouraged and inspired me during difficult times. I cannot express enough how thankful I am to be the daughter of the most wonderful parents. I thank my parents for teaching me that I can do all things through Christ who gives me strength. I am extremely grateful for my family and friends in God's grace. I dedicate this thesis to my family.

## Table of Contents

Chapter 1. Introduction/Background .....	1
1.1 Polymer in Semiconductor Industry.....	1
1.2 Chemical Shrinkage and Modulus Evolution.....	1
Chapter 2. Background: Usage of Fiber Bragg Grating Sensor to Measure Curing Properties Evolutions .....	5
2.1 Fiber Bragg Gratings as a Strain Sensor .....	5
2.2 Governing Equation to Measure Property Evolutions with FBGs Embedded in Cylindrical Polymer Substrate .....	8
2.3 Specimen Configuration.....	11
2.4 Procedure to Determine Property Evolutions.....	11
2.5 Implementation with Convection Oven .....	14
Chapter 3. Motivation/Objective .....	15
3.1 Heat Generation during Polymerization.....	16
3.2 Temperature Controllability of the System.....	20
3.3 Other Challenges Associated with the Previous System.....	22
Chapter 4. Proposed Approach.....	25
4.1 FBG on Special Fiber.....	25
4.2 Conduction Heater as Heating Source .....	29
4.3 Design Requirements of the Proposed System .....	33
4.4 Design Specifications of the Proposed System .....	34
Chapter 5. Implementation/ Experiment Procedure .....	42
Chapter 6. Results and Discussion .....	45
6.1 Temperature Profile of the Proposed System.....	45
6.2 BW Data for Two Configurations .....	47
6.3 Gelation Point Determination and Deformed BW Data.....	50
6.4 Step Size Input and Calculations of Effective Chemical Shrinkage and Modulus Evolutions.....	53
Chapter 7. Conclusions.....	54
Appendix.....	57
References.....	60

## List of Figures

Figure 1. Illustration of (a) an FBG and corresponding spectrum and (b) BW shift [12] ..	6
Figure 2. Schematic diagram of an FBG sensor embedded in a cylindrical substrate [12]	8
Figure 3. Illustration of BW shifts and the segment division of two configurations [12]	13
Figure 4. Schematic illustration of Wang's experimental setup [12] .....	15
Figure 5. Temperature profile of a cylindrical polymer during curing [12] .....	17
Figure 6. Curing extent evolution of a cylindrical polymer during the curing [12] .....	18
Figure 7. Maximum curing extent difference of various C-1 configurations (a) total exotherm, $\Delta H=200J/g$ ; (b) $\Delta H=400J/g$ [24].....	20
Figure 8. Typical temperature response of convection oven used for previous system ...	21
Figure 9. (a) BW shift data of 25.4x UF-2 specimen with 30mm length, (b) Schematic of friction force against shrinkage during curing of polymer specimen .....	23
Figure 10. Full spectrum of two UF-2 specimens A and B .....	24
Figure 11. Intrinsic BW data of FBG's on (a) 125 $\mu m$ cladding diameter fibers and (b) 80 $\mu m$ and 175 $\mu m$ cladding diameter fibers .....	27
Figure 12. Specimen Configurations with Different Fiber Diameter .....	29
Figure 13. (a) Conduction Heater and (b) Controller .....	30
Figure 14. (a) Transient Temperature Analysis Result of the Proposed System, (b) temperature analysis figure .....	32
Figure 15. Basic concept of the proposed design .....	33
Figure 16. Detailed concept of the proposed design.....	34

Figure 17. Design illustration of proposed system .....	35
Figure 18. Optimized metal mold designs (a) Bottom mold, (b) Top mold, and (c) Bottom and Top mold assembly .....	37
Figure 19. Fiber alignment system of the proposed system; (a) fiber holders assembled on fiber alignment fixture with bottom mold, and (b) top mold assembled to (a).....	38
Figure 20. Final proposed design; (a) Machine design of overall structure, (b) Machine design close-up, and (c) Machined parts assembled.....	42
Figure 21. Assembled metal molds and silicone rubber tube .....	43
Figure 22. Fiber alignment using RTV .....	44
Figure 23. Injection of polymer in tilted system.....	44
Figure 24. Temperature profile of polymer during polymerization in (a) Convection oven and (b) Conduction heater.....	46
Figure 25. BW Shift data of 25.4x UF-2 specimens with 30mm and 15mm lengths .....	48
Figure 26. (a) Raw BW data of two UF-2 specimens recorded during polymerization (b) First 55 minutes after heating started.....	49
Figure 27. (a) Raw BW data loaded for both configurations C-1 and C-2, (b) Determination of gelation point for both configurations .....	51
Figure 28. (a) Deformed BW data of both configurations, C-1 (125um FBG) and C-2 (80um FBG), (b) Fitted data .....	52
Figure 29. Evolution properties of UF-2 (1) effective chemical shrinkage, and (2) modulus.....	54

## **Chapter 1.      Introduction/Background**

### **1.1 Polymer in Semiconductor Industry**

Use of polymer in semiconductor industry is considered very critical in all aspects of semiconductor package, such as the packaging, the interconnections, and the encapsulations for protecting the chips and interconnections from the environment. The selection of polymer has a great influence on the reliability and performance of an electronic system, and therefore, advanced material considerations can lead to more demanding packaging schemes. [1]

There are different material properties to be considered when selecting polymeric materials, such as curing evolutions, Coefficient of Thermal Expansion, Visco-elastic properties, etc. In this study, a technique to accurately measure curing evolution properties of polymeric materials is proposed. During curing, it is important to characterize effective chemical shrinkage evolution and modulus evolution, which will be critical especially during manufacturing process of electronic packages.

### **1.2 Chemical Shrinkage and Modulus Evolution**

Polymeric materials are composed of molecules with very high molecular weight and they can be divided into three categories: thermoplastic, thermoset, or elastomer [2]. Thermosetting polymers, which are mostly used in electronic packaging, are cross-linked and solidify by being cured chemically where the long chains of molecules become cross-linked with each other. During the chemical curing process, volumetric shrinkage of a

thermosetting polymer occurs as the distance between molecules move decreases from a van der Waals distance of separation to a distance of covalent bonding. This shrinkage caused by curing is called chemical shrinkage, which can be quantified using the specific volume change,  $\nu^{ch}$ , defined as

$$\nu^{ch} = \frac{\Delta V}{V_0} \quad (1)$$

where  $\Delta V$  is the volume change during the curing and  $V_0$  is the original volume before polymerization. It is known that the specific volume shrinkage can be between 10% and 20% depending on the chemical composition and the polymerization reaction of polymers [3]. The term *chemical shrinkage strain* can be more useful in mechanical modeling and can be expressed in terms of specific volume shrinkage as [4]

$$\varepsilon^{ch} = \sqrt[3]{1 + \nu^{ch}} - 1 \quad (2)$$

where  $\varepsilon^{ch}$  is the chemical shrinkage strain and  $\nu^{ch}$  is specific volume shrinkage. As a mechanical strain, the chemical shrinkage can generate residual stresses during curing of polymeric materials. The residual stresses developed in packages can be considered negligible when cured at high temperatures due to the small modulus of polymers [5-7]. On the other hand, the modulus of cured polymers can be large enough to cause considerable residual stresses when cured at low temperature, especially below  $T_g$ , and therefore, chemical shrinkage should be characterized.

Chemical shrinkage can also affect the functionality. For example, electrical conductivity of adhesives that contain polymeric matrices and conductive fillers is usually low before curing but increases when cured. Conductivity increases during curing because the shrinkage of polymer binder causes close contact of conductive fillers.

[8] Therefore, increasing the chemical shrinkage of a polymer matrix can improve electrical conductivity of adhesives.

Another important mechanical property to consider is the modulus,  $E$ , which quantifies stiffness, the resistance of a material to mechanical deformation, and the ability to store deformation energy. The modulus of polymers evolves during the polymerization process which is a dynamic process as polymers in liquid or gel state gradually solidify at the curing temperature in general. This means that the modulus evolves from virtually zero at the gelation point to a final value at the end of curing, and the knowledge of not only the final modulus, but also the modulus evolution is required in order to predict the residual stresses induced by polymerization. Theoretically, it is generally hypothesized that an increment of curing induced strain,  $d\varepsilon$ , contributes to the stress after completion of the process according to Hooke's law [9]. Stress increment can be calculated as follows in case of uni-axial condition,

$$d\sigma = E(t)d\varepsilon \quad (3)$$

where  $E$  is the modulus at the time of the strain increment. The total stress  $\sigma$  can be obtained by integrating Equation (3) over the curing process

$$\sigma = \int E(t)d\varepsilon \quad (4)$$

As shown in Equation (4), quantifying curing induced residual stress requires evolution of the modulus. Although it can be practically difficult, it is important to understand and measure the chemical shrinkage and modulus evolution for development of new polymers and improvement of the performance of electronic packaging products.

Most methods that measure chemical shrinkage can only quantify the total (intrinsic) chemical shrinkage, and cannot detect gelation point. Gelation point can be defined as a conversion point at which an infinite molecular network is formed [10], and where the polymer has apparent elastic properties [11]. Consequently, only chemical shrinkage after gelation point should be used when characterizing the curing induced residual stresses in the assembly, instead of the total chemical shrinkage. This portion of total chemical shrinkage that contributes to accumulation of residual stresses is defined as “*effective chemical shrinkage*.” [12]

Since most of the methods focus on the measurement of total shrinkage, and no efficient method was found to be able to determine the chemical shrinkage evolution as well as the gelation point, Yong Wang and Bongtae Han at the University of Maryland proposed a method that utilizes a Fiber Bragg Grating sensor to measure the effective chemical shrinkage and modulus evolutions during curing of polymeric materials. Wang developed this technique that uses the FBG sensor as a strain sensor to measure the Bragg wavelength shift of two different specimens of different configurations which are later converted to chemical shrinkage and modulus evolutions. This method is the core technique of which this paper is based on, and will be discussed in details in the following chapter.

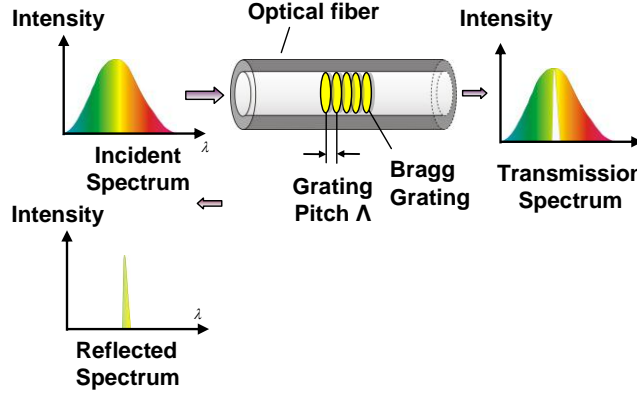
## Chapter 2. Background: Usage of Fiber Bragg Grating Sensor to Measure Curing Properties Evolutions

### 2.1 Fiber Bragg Gratings as a Strain Sensor

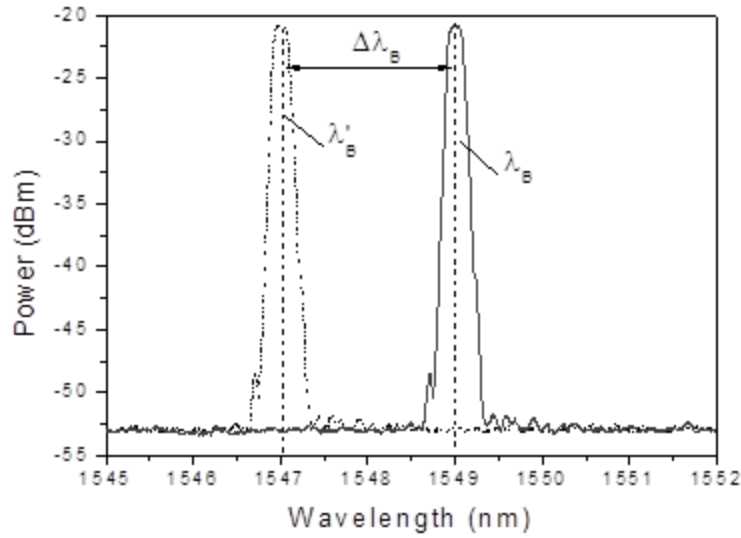
In the method proposed by Yong Wang, a fiber Bragg grating was used as a strain sensor, which is named for William Lawrence Bragg who formulated the conditions for X-ray diffraction which relate energy spectra to reflection spacing (Bragg's Law). A fiber Bragg grating is made by a periodic perturbation of refractive index along the fiber length which is typically created by exposing the fiber core to an intense interference pattern of UV energy.[13-15] When a band of the incident light encounters a material with higher index of refraction, one of the periodic gratings, some of the incident light is reflected, some is refracted, and some is transmitted. As shown in Figure 1 (a), the Bragg grating allows a portion of the incident light to be reflected at certain wavelength (known as the Bragg wavelength) that satisfies

$$\lambda_B = 2n_{eff}\Lambda \quad (5)$$

where  $\lambda_B$  is the Bragg wavelength,  $n_{eff}$  is the effective refractive index and  $\Lambda$  is the grating pitch.



(a)



(b)

Figure 1. Illustration of (a) an FBG and corresponding spectrum and (b) BW shift [12]

Since each grating serves to reflect a portion of the input light signal, the amount of the light reflected at the Bragg wavelength is dependent on the perturbation of refractive index,  $\Delta n$ , as well as the total grating length. Figure 1 (b) illustrates shift in the Bragg wavelength caused by external disturbances such as changes in temperature or strain that will change the grating pitch and effective refractive index of the FBG, which becomes the basic principle of using FBGs as a sensor.

Differentiating Eqn. (5) yields [13-15],

$$\frac{\Delta\lambda_B}{\lambda_B} = \frac{\Delta\Lambda}{\Lambda} + \frac{\Delta n_{eff}}{n_{eff}} = \varepsilon_1 + \frac{\Delta n_{eff}}{n_{eff}} \quad (6)$$

where  $\Delta\Lambda$  and  $\Delta n_{eff}$  are the changes in the grating pitch and the effective refractive index, respectively, and  $\varepsilon_1$  is the axial strain along the fiber. For isotropic and straight Bragg grating, it can be obtained as [16]

$$\Delta n_{eff} = -\frac{n^3}{2} \left[ P_{12}\varepsilon_1 + (P_{11} + P_{12})\varepsilon_2 - \left\{ \frac{2}{n^3} \frac{dn}{dT} + (P_{11} + 2P_{12})\alpha_f \right\} \Delta T \right] \quad (7)$$

where  $\varepsilon_2$  is the transverse strain,  $P_{ij}$  are strain-optic coefficients (Pockel's coefficients),  $\frac{dn}{dT}$  is the thermo-optic coefficient,  $\alpha_f$  is the CTE of the fiber core material, and  $\Delta T$  is the temperature change with respect to the initial condition.

In case of uni-axial loading condition where  $\varepsilon_2 = -\nu\varepsilon_1$  and there is zero temperature change, Eqns. (6) and (7) can be simplified to

$$\Delta\lambda_B = \lambda_B(1 - P_k)\varepsilon_1 \quad (8)$$

where  $P_k$  is called “*effective strain-optic constant*”, defined as

$$P_k = -\frac{n^2}{2} \left[ P_{12} - \nu(P_{11} + P_{12}) \right] \quad (9)$$

where  $\nu$  is the Poisson's ratio of the fiber material.

It can be seen that the axial strain is linearly proportional to the Bragg wavelength shift in Equation (8). FBGs are widely used as strain sensors in practice, and were used in Wang's method to characterize properties of polymer substrates as well.

## 2.2 Governing Equation to Measure Property Evolutions with FBGs Embedded in Cylindrical Polymer Substrate

In this section, Wang's method to measure chemical shrinkage and modulus evolution properties of polymeric materials during curing will be discussed. Wang developed the method based on using the Fiber Bragg Grating sensor of an outer radius of  $a$ , embedded in a cylindrical polymer matrix that has an inner radius of  $a$ , and an outer radius of  $b$ . A schematic drawing of the FBG and the matrix is shown in Figure 2.

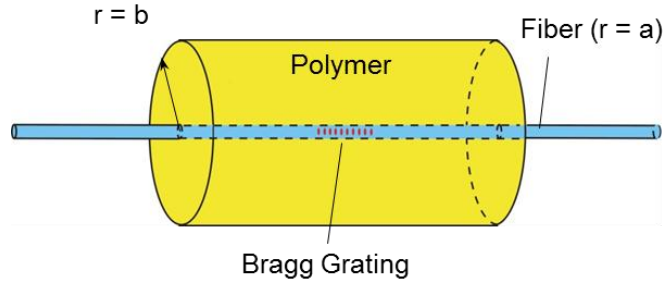


Figure 2. Schematic diagram of an FBG sensor embedded in a cylindrical substrate [12]

When modeling the behavior of an FBG embedded in a matrix, Eqn. (8) has been widely used. This equation states that the change in Bragg wavelength, or Bragg wavelength shift, is linearly proportional to the axial strain applied to the fiber. However, when FBG is embedded, the actual loading applied to the FBG is three dimensional. Wang's analytical solution will be presented in this section for an FBG's response when it is embedded in a cylindrical polymer substrate.

Any type of loading can be applied to FBG and induce Bragg wavelength shift of an FBG. By combining Eqns. (6) and (7), the BW shift can be written as

$$\frac{\Delta\lambda_B}{\lambda_B} = \varepsilon_1 - \frac{n^2}{2} \left[ P_{12}\varepsilon_1 + (P_{11} + P_{12})\varepsilon_2 - \left\{ \frac{2}{n^3} \frac{dn}{dT} + (P_{11} + 2P_{12})\alpha_f \right\} \Delta T \right] \quad (10)$$

Where  $\varepsilon_1$  and  $\varepsilon_2$  are the axial and transverse strains respectively,  $P_{ij}$  are strain-optic coefficients,  $\frac{dn}{dT}$  is the thermo-optic coefficient,  $\alpha_f$  is the CTE of the fiber core material, and  $\Delta T$  is the temperature change. When the thermal loading and mechanical loading coexist, the strain components can be expressed as

$$\varepsilon_1 = \varepsilon_1^\sigma + \alpha_f \Delta T \quad (11)$$

and

$$\varepsilon_2 = \varepsilon_2^\sigma + \alpha_f \Delta T \quad (12)$$

where  $\varepsilon_1^\sigma$  and  $\varepsilon_2^\sigma$  are the stress-induced axial strain and transverse strain of the fiber, respectively. Substituting Equations (11) and (12) into Equation (10) yields

$$\Delta\lambda_B = \lambda_B \left( \alpha_f + \frac{1}{n_{eff}} \frac{dn}{dT} \right) \Delta T + \left\{ \varepsilon_1^\sigma - \frac{n^2}{2} [P_{12}\varepsilon_1^\sigma + (P_{11} + P_{12})\varepsilon_2^\sigma] \right\} \lambda_B = \Delta\lambda_B^i + \Delta\lambda_B^d \quad (13)$$

where  $\Delta\lambda_B^i$  is called “*intrinsic*” BW shift which is defined as

$$\Delta\lambda_B^i = \lambda_B \left( \alpha_f + \frac{1}{n_{eff}} \frac{dn}{dT} \right) \Delta T \quad (14)$$

and  $\Delta\lambda_B^d$  is called “*deformation*” induced BW shift which is defined as

$$\Delta\lambda_B^d = \left\{ \varepsilon_1^\sigma - \frac{n^2}{2} [P_{12}\varepsilon_1^\sigma + (P_{11} + P_{12})\varepsilon_2^\sigma] \right\} \lambda_B \quad (15)$$

The name “*intrinsic*” is given to  $\Delta\lambda_B^i$  where this BW shift is not associated with any stress-induced deformation. [12]

In Equation (15),  $\varepsilon_1^\sigma$  and  $\varepsilon_2^\sigma$  are mechanical strains which can be derived for a given mechanical load using the theory of elasticity. Referring back to Wang’s

configuration where the FBG with outer radius of  $a$  is embedded in the cylindrical polymer matrix that has an inner radius of  $a$  and an outer radius of  $b$ , a loading condition of a piecewise constant temperature distribution can be defined as

$$T(r) = \begin{cases} T_f, & 0 \leq r < a \\ T_s, & a < r \leq b \end{cases} \quad (16)$$

where  $T_f$  and  $T_s$  are the *pseudo temperature change* of the fiber and the substrate from the reference temperature, respectively. The piecewise constant temperature condition is introduced to evaluate chemical shrinkage which can be simulated as thermal contraction by analogy. [12]

It is necessary to assign different “pseudo-temperature” changes in each material since strain due to chemical shrinkage is different in each material, as tendency to shrink is proportional to the temperature change in this analogy. Under the assumption of the generalized plane strain condition, where the axial strain is an unknown constant, the analytical solution of the stress components can be derived. The formulations are shown in the Appendix - A, where the subscripts,  $f$  and  $s$ , represent the fiber and substrate parameters, respectively.[12] Wang verified the derived analytical solution by a 2-D axisymmetric finite element model.

Wang then derived the relationship between the stress components and the “*deformation*” induced BW shift as

$$\Delta\lambda_B^d = \frac{1}{E_f} \left\{ \left[ 1 - \frac{n^2}{2} (P_{12} - (P_{12} + P_{11})\nu_f) \right] \sigma_{zz}^f - \left[ 2\nu_f + \frac{n^2}{2} ((1-\nu_f)P_{11} + (1-3\nu_f)P_{12}) \right] \sigma_{rr}^f \right\} \lambda_B \quad (17)$$

This equation represents an analytical relationship between the “deformation induced” BW shift and the material properties of the polymer substrate under the loading condition shown in Equation (16). [12]

## 2.3 Specimen Configuration

After the governing equation was established, Wang conducted some analysis on understanding sensitivity of the deformation induced BW shift to (1) outer radius of polymer,  $b$ , and (2) Poisson’s ratio of polymer,  $\nu_s$ . Wang analyzed that if  $b/a$  is greater than 200, the behavior of the assembly will be governed by polymer to do high volume stiffness, defined by volume multiplied by modulus, however, this is not valid due to heat generation during polymerization as it will be discussed in the later part of this paper. Wang concluded that it is required to use small size configuration of polymer in order to minimize the heat generation during polymerization [12].

Wang also concluded that the BW shift is independent of the Poisson’s ratio of polymer substrate and only depends on polymer substrate’s shrinkage strain and modulus, and therefore, 2 different specimen configurations are required in order to solve for 2 unknowns: shrinkage strain and modulus [12].

## 2.4 Procedure to Determine Property Evolutions

In this section, the procedure to determine property evolutions using measured BW data that was developed by Wang is discussed. Assuming that a shrinkage strain of  $\Delta\varepsilon^{ch}$  occurs in the polymer substrate, the loading condition can be written as

$$\varepsilon(z) = \begin{cases} 0 & \text{for } 0 \leq r < a \\ \Delta\varepsilon^{ch} & \text{for } a < r \leq b \end{cases} \quad (18)$$

where  $a$  is the radius of the FBG and  $b$  is the outer radius of the polymer substrate. The thermal analogy, Equation (16), can be written as

$$T(r) = \begin{cases} 0, 0 \leq r < a \\ \frac{\Delta\varepsilon^{ch}}{\alpha_s}, a < r \leq b \end{cases} \quad (19)$$

where  $\alpha_s$  is the CTE of the polymer which can be set as an arbitrary number. Analytical solution of the stress fields within the FBG (Equation (17)) is shown in the Appendix – A at the end of this paper, and the governing equation will take a form of

$$\Delta\lambda_B^d = F(E_s, \beta) \cdot \Delta\varepsilon^{ch} \quad (20)$$

where  $E_s$  is an instant modulus of polymer substrate,  $\beta = \frac{b}{a}$ , and  $F$  is a nonlinear function of  $E_s$  and  $\beta$ . Since there are two unknown constants (effective chemical shrinkage and modulus) in the governing Equation (20), the BW shifts are measured for two different specimen configurations to determine the constants which are referred to as C-1 and C-2 with  $\beta = \beta_1$  and  $\beta_2$ , respectively. Typical results of the measured BW shifts in the two configurations are illustrated schematically in Figure 3. [12]

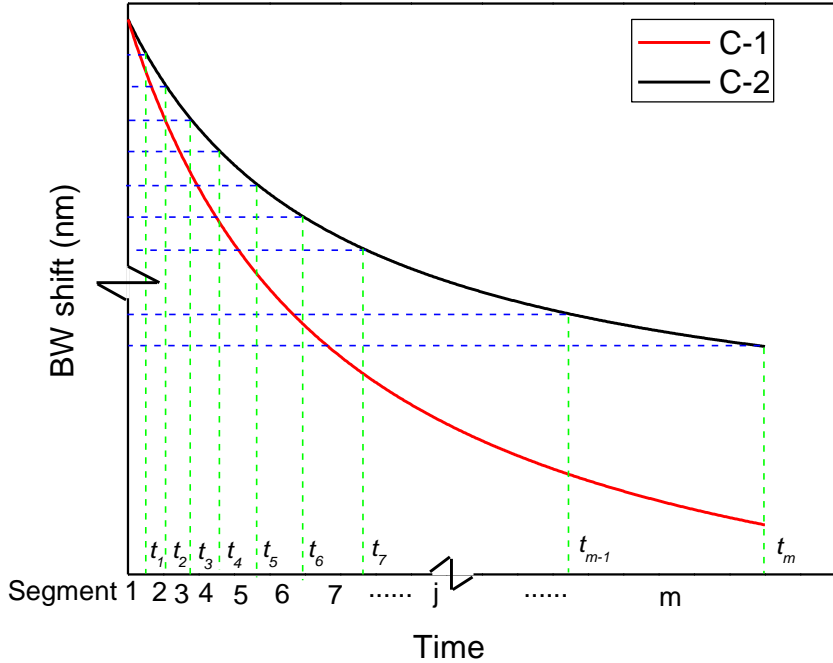


Figure 3. Illustration of BW shifts and the segment division of two configurations [12]

During polymerization, the effective chemical shrinkage and modulus evolve with time, and are determined incrementally by dividing the entire curing history into  $m$  numerous small time segments. The BW shift of C-2 where  $\beta_2 < \beta_1$  in each segment is even after the division, and the BW shift increments of C-1 and C-2 in the  $j^{\text{th}}$  ( $j = 1$  to  $m$ ) segment are called  $\Delta\lambda_{B1,j}$  and  $\Delta\lambda_{B2,j}$  respectively. The governing Equation (20) can develop the following simultaneous equations of the two configurations C-1 and C-2.

$$\begin{cases} \Delta\lambda_{B1,j} = F(E_{s,j}, \beta_1) \cdot \Delta\varepsilon_j^{ch} \\ \Delta\lambda_{B2,j} = F(E_{s,j}, \beta_2) \cdot \Delta\varepsilon_j^{ch} \end{cases} \quad (21)$$

The shrinkage increment  $\Delta\varepsilon_j^{ch}$  is eliminated when dividing the first equation by the second equation in Equation(21), and the instant equilibrium modulus  $E_{s,j}$  is determined

by solving the nonlinear equation. Then the  $E_{s,j}$  can be substituted back into one of the two equations to calculate  $\Delta\varepsilon_j^{ch}$ . [12]

The above procedure is repeated when  $m$  increases until the convergence is achieved. It is important to note that the result of effective chemical shrinkage is in an accumulated manner while the result of the modulus is instantaneous. Specimen configurations were also determined as well as the length of the specimen, which is also important, so that the generalized plane strain condition is achieved. [12]

## 2.5 Implementation with Convection Oven

Wang's set up utilized convection oven as heating source. Silicone rubber tube was used to cure polymer in a cylindrical shape, which was held by teflon molds designed to hold the silicone rubber tube and the fiber inside the convection oven. The diameter of the FBG used in the experiment is  $125 \mu m$ . Considering the practicality and commercial availability of silicone rubber tubes, in this study, the inner diameter of the tube is  $3/16''$  in specimen configuration C-1 and  $3/32''$  in configuration C-2; which leads to  $\beta_1 = 38$  and  $\beta_2 = 19$ . The total length of Bragg gratings and the length of the polymer specimen are 5 mm and 50 mm, respectively [12]. The following procedure was used to fabricate a specimen:

1. Place an FBG through a silicone rubber tube;
2. Secure the FBG along the groove of the Teflon base;
3. Assemble the bottom Teflon cap;
4. Inject a polymer of interest into the tube;

5. Embed a fine-wire thermal couple;
6. Assemble the top Teflon cap;
7. Place the molds inside convection oven;
8. Cure the polymer.

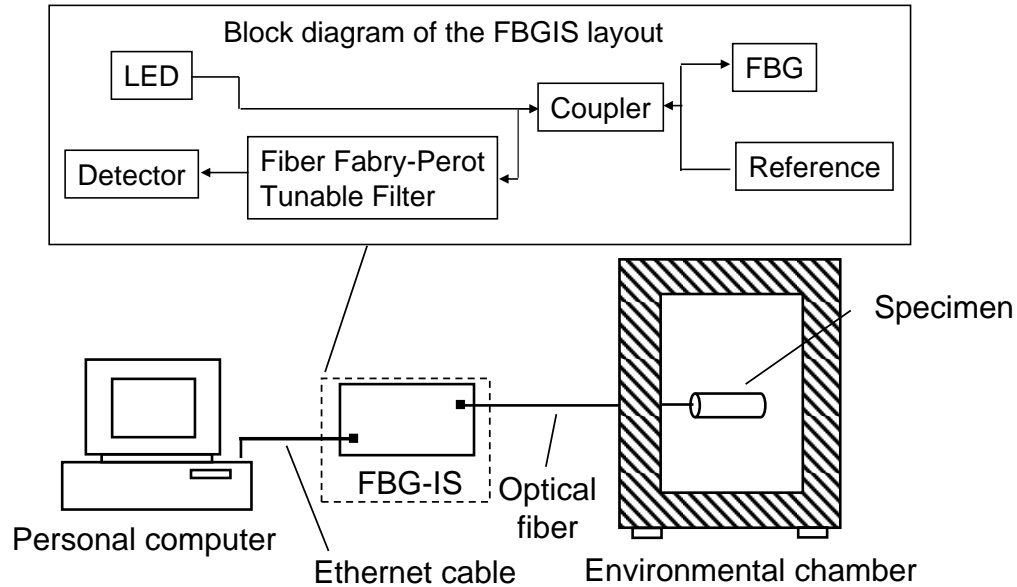


Figure 4. Schematic illustration of Wang's experimental setup [12]

The figure above illustrates how the wavelength is recorded during the experiment. The specimen is placed inside environmental chamber for curing, and the fiber is connected to an Interrogator (FBG-IS) which sends signal to the personal computer.

### Chapter 3. Motivation/Objective

Even though Wang's method was theoretically well established, there were some challenges associated in implementation stage that needed to be addressed and modified

with improvements. In this chapter, major challenges in the aspect of implementation will be addressed and discussed in details.

### 3.1 Heat Generation during Polymerization

The biggest challenge associated with the previous system involves heat generation of polymeric material as curing proceeds. Polymerization is an exothermic process where the temperature can rise considerably, especially in bulk materials. The Fourier's heat conduction equation for a cylindrical shape specimen with radius  $r$  of  $b$  and has the form

$$k \left( \frac{\partial^2 T}{\partial r^2} + \frac{1}{r} \frac{\partial T}{\partial r} \right) + \dot{q} = \rho c_p \frac{\partial T}{\partial t} \quad (22)$$

where  $k$  is the thermal conductivity,  $T$  is the temperature,  $t$  is the time,  $\rho$  is the density,  $c_p$  is the specific heat and  $\dot{q}$  is the heat generation rate. The heat generation during polymerization is directly related to the reaction speed through the equation [12]

$$\dot{q} = \rho \Delta H \frac{dp}{dt} \quad (23)$$

where  $p$  is the curing extent and  $\Delta H$  is the total exotherm of the reaction. For simplicity, the polymerization can be modeled by an  $n^{\text{th}}$  order model [17-23]

$$\frac{dp}{dt} = k_c (1-p)^n \quad (24)$$

where  $k_c$  is a temperature-dependent rate coefficient and it is related to the temperature through Arrhenius's equation

$$k_c = A e^{-\frac{E_a}{RT}} \quad (25)$$

where  $A$  is a material constant,  $E_a$  is the activation energy and  $R$  is the ideal gas constant, which is  $8.314 \text{ J/mol}\cdot\text{K}$ . Wang developed the thermal modeling of polymerization process using boundary conditions of his convection oven system using ANSYS, where he predicted the temperature overshoot of the case  $b/a = 200$  when cured at temperature  $165^\circ\text{C}$  as shown in Figure 5.

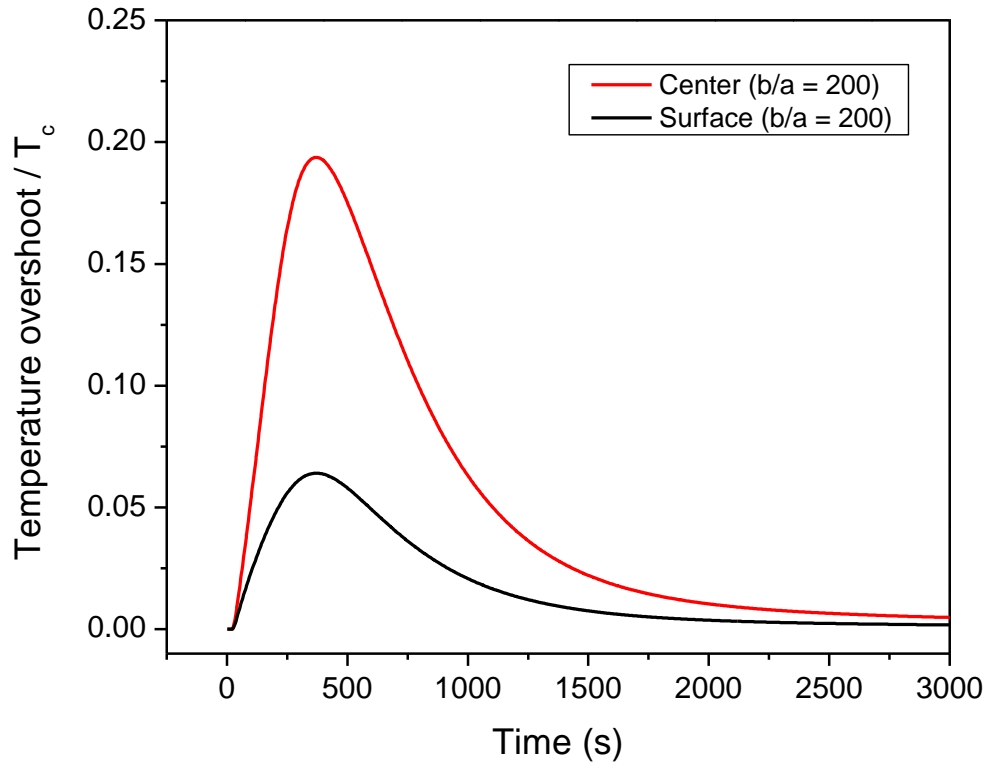


Figure 5. Temperature profile of a cylindrical polymer during curing [12]

It was found that the center temperature showed significant overshoots by  $0.2T_c$  at the maximum. This can cause large temperature gradient in the material, and partial curing which will cause large thermal strain on the embedded FBG while the temperature is dropping back to  $T_c$  that will be incorporated with the chemical shrinkage measured

during curing. This can be also explained using curing extent evolutions, shown in Figure 6.

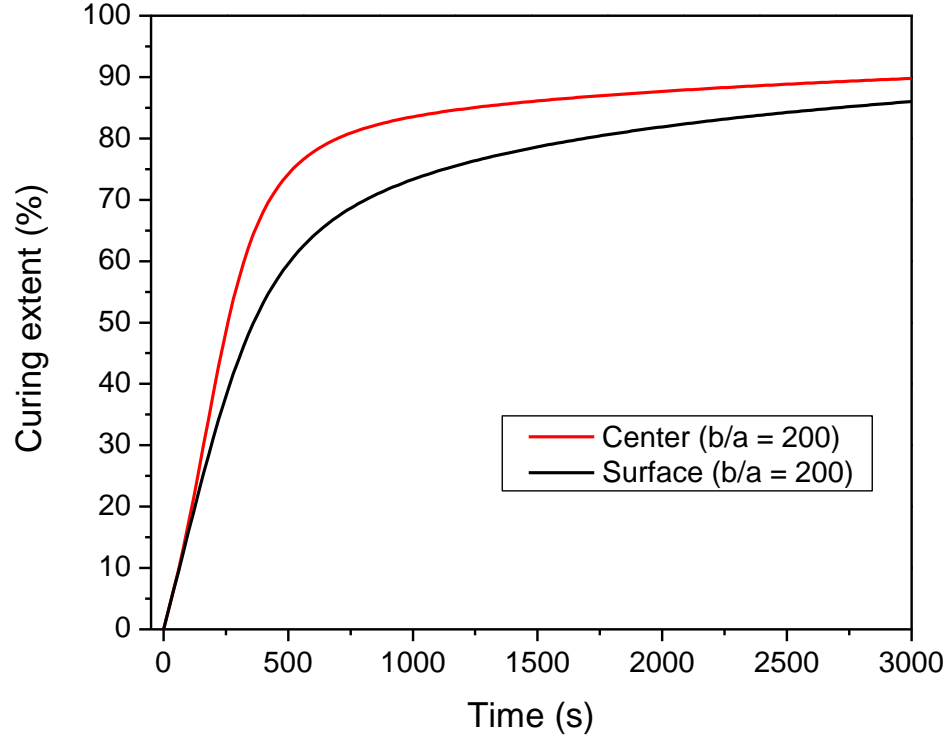
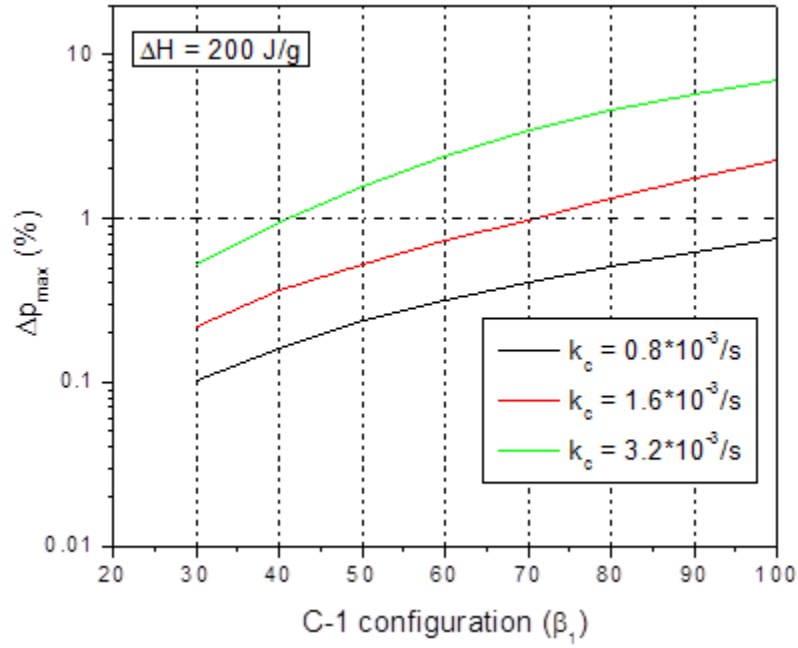


Figure 6. Curing extent evolution of a cylindrical polymer during the curing [12]  
This plot illustrates that the bulk specimen should not be used in the analysis and  
the FBG sensor should be embedded in polymers of small size to avoid problems  
associated with heat generation during polymerization.

Wang selected specimen configurations of  $\beta_1 = 19$  and  $\beta_2 = 38$  to obtain maximum sensitivity while minimizing heat generation as much as possible. Especially from the bigger configuration, due to larger volume of material trapped inside the silicone rubber tube which is an insulating material, heat generated during curing had no route to escape and therefore increased the temperature at the center of polymer significantly. He also conducted numerical analysis to examine the maximum curing extent difference

between the center of C-1 and the surface of C-2,  $\Delta p_{max}$ . A wide range of the total exotherm,  $\Delta H$ , and the curing rate coefficient,  $k_c$ , was considered in this numerical analysis in order to cover most of the thermosetting polymers used in semiconductor packaging applications. The simulation results are shown below.



(a)

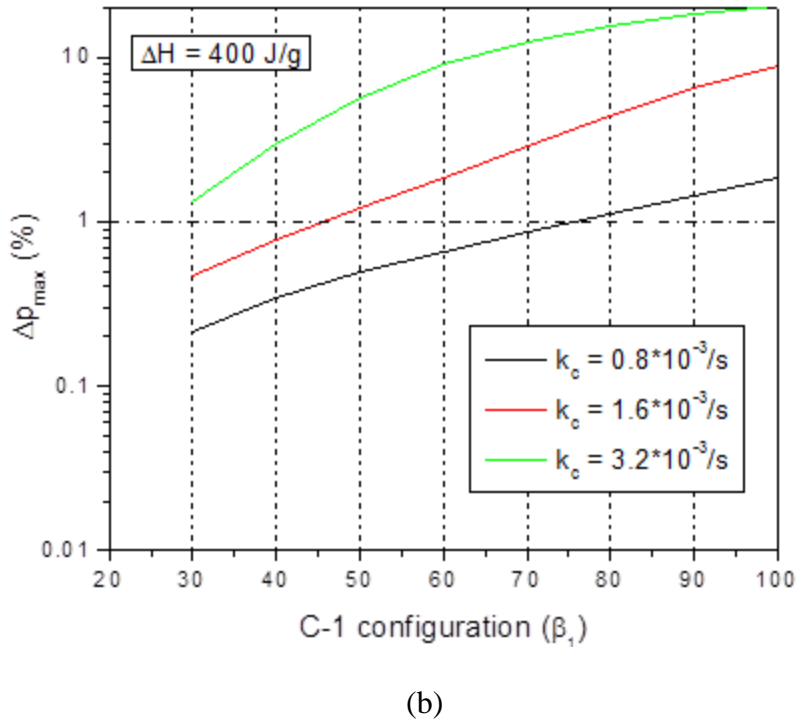


Figure 7. Maximum curing extent difference of various C-1 configurations (a) total exotherm,  $\Delta H=200J/g$ ; (b)  $\Delta H=400J/g$  [24]

In Figure 7 (a), it can be concluded that the maximum curing extent difference of low total exotherm polymer for entire range of curing rate coefficients shows less than 1% for C-1 of  $\beta_1=40$ . However, polymer with high total exotherm shown in Figure 7 (b) shows more than 1% difference especially for the high curing rate coefficient. Certain polymers with low heat generation rate during polymerization may be characterized using previous system, however, polymers with high exotherm and curing rate coefficient will not be ideal for the previous system.

### 3.2 Temperature Controllability of the System

Another major challenge was associated with the heating source, the environmental convection oven. With the convection oven, temperature controllability

and system accessibility were very limited. Because it uses air/liquid nitrogen to heat/cool the specimen, heating/cooling ramp rates were too low, and the stabilization of temperature was not easily controllable. Temperature response was also very slow because the oven had to heat/cool the entire volume of air within the control volume defined by the oven. The plot below shows typical response of temperature control within convection oven used for previous system using its own temperature control program called PID3.

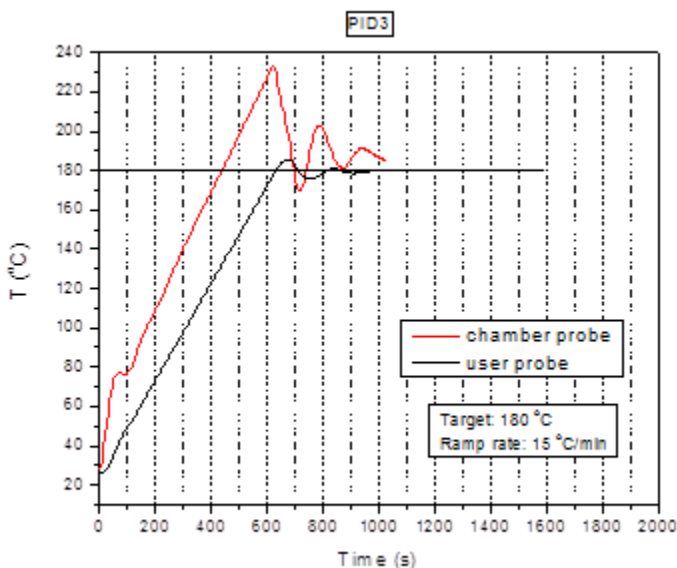


Figure 8. Typical temperature response of convection oven used for previous system

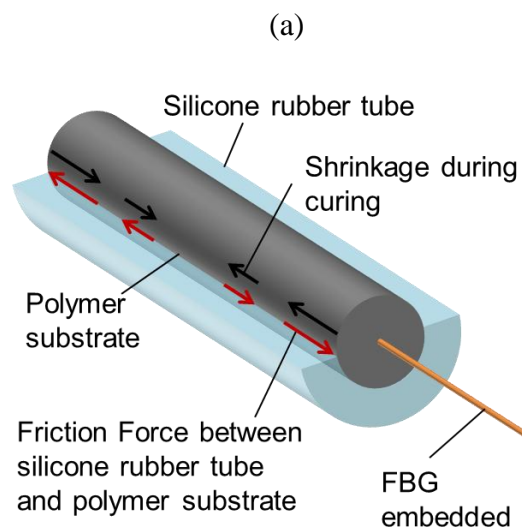
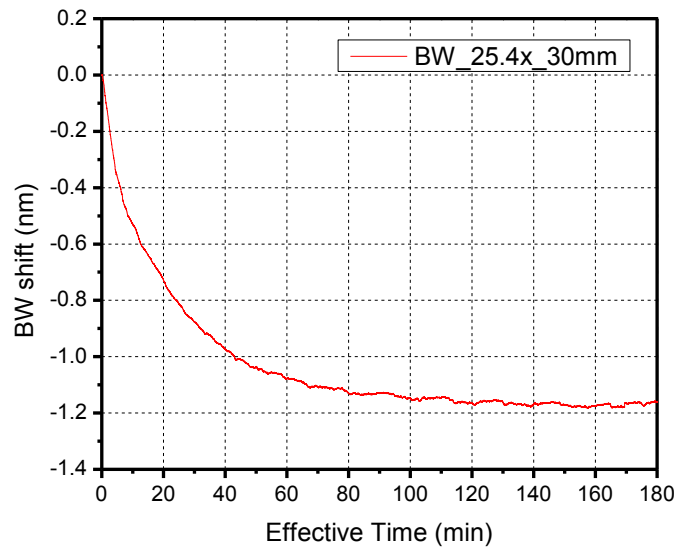
This particular temperature plot shows temperature response of a polymer specimen with diameter of 5mm and length of 60mm. Chamber probe was used to record the temperature of air inside convection oven, and the user probe was used to measure the temperature of the polymer specimen. It can be easily seen that the temperature control and stabilization are complicated and limited using the convection oven.

Additionally, due the fact that the air within control volume had to be isolated from environment during heating/cooling, accessibility to the system during test was very limited. It is also important that the temperature should be stabilized before curing starts to happen, however, if not, it is very hard to clearly determine where the gelation point is. This can also cause error in determination of curing property evolutions since BW shift will include not only the strain due to curing but also thermal strain as the temperature of the specimen changes.

For the combined reasons, it was challenging to test two configurations simultaneously. Due to heat generation, temperature overshoot was typical, and the temperature response of the convection oven was too slow to control the temperature of specimen quickly and precisely.

### 3.3 Other Challenges Associated with the Previous System

Friction inside the silicone rubber tube was another concern. Even though silicone rubber has very small modulus, the friction force between the outer surface of polymer and inner surface of silicone rubber tube could not be ignored. The friction can introduce constrain to the polymer as it starts to shrink during curing, which will not allow the polymer to deform freely due to shrinkage during curing as shown below in Figure 9 (b). The data below shows BW shift data taken after gelation point of curing underfill material called UF-2 of a specimen with length of 30mm.



(b)

Figure 9. (a) BW shift data of 25.4x UF-2 specimen with 30mm length,  
(b) Schematic of friction force against shrinkage during curing of polymer specimen

In Figure 9 (a), it can be clearly seen that the BW data fluctuates as it drops during polymerization. The physical behavior of the polymer during polymerization can cause this type of fluctuation. Since the polymer was constrained due to friction between the

tube and polymer surface, the polymer was constrained during shrinkage and did not shrink freely and smoothly.

The fiber alignment was also another important issue to be addressed. The following plot shows full reflected spectrums of two specimens after polymer was cured around FBG sensors.

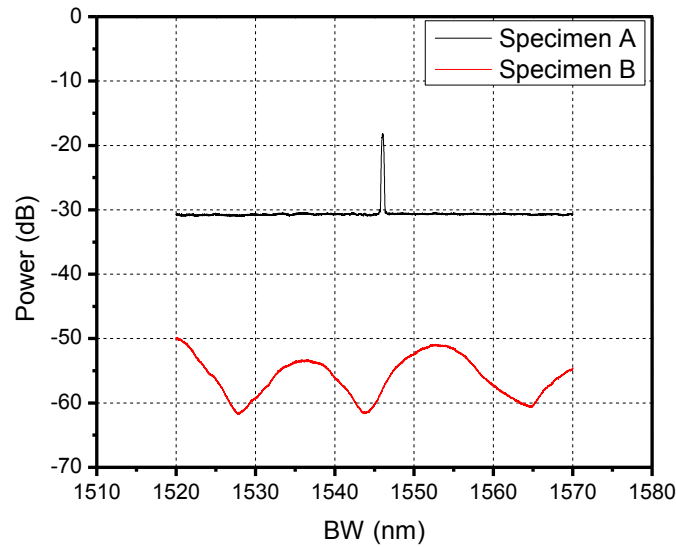


Figure 10. Full spectrum of two UF-2 specimens A and B

As shown in Figure 10, Specimens A and B do not exhibit same or similar full reflected spectrums. Specimen A shows normal behavior whereas the Specimen B shows peculiar behavior. Such disrupted response can be caused by many different reasons. Critical causes that should be considered in this FBG system can be micro-bending of fiber and un-uniform curing of polymer around FBG sensor area. Micro-bending of fiber around the FBG sensor area can cause significant loss due to the bend, disrupting the wave guidance of the light in the core because the light tends to travel in a straight line. Non-uniform curing of polymer around FBG sensor area can also disturb the spectrum

because it can apply uneven force to the fiber. The uniformly spaced grating within fiber will no longer be uniformly spaced and cause such disturbance of the reflected spectrum. Non-uniform curing of polymer can occur when temperature of the polymer substrate is not uniform. Since the configuration of the polymer substrate is only 3.175mm in diameter and is well buried inside the silicone rubber tube, temperature uniformity should not be a problem. This was also confirmed with thermal analysis as shown in section 4.2 where it only shows less than 0.3°C temperature distribution within the polymer substrate. However, micro-bending can easily occur when the fiber is poorly aligned. Fiber should be aligned with precision in order to ensure that the fiber is located at the center of the polymer substrate and is maintained straight with no bending especially around the FBG sensor area.

## **Chapter 4.      Proposed Approach**

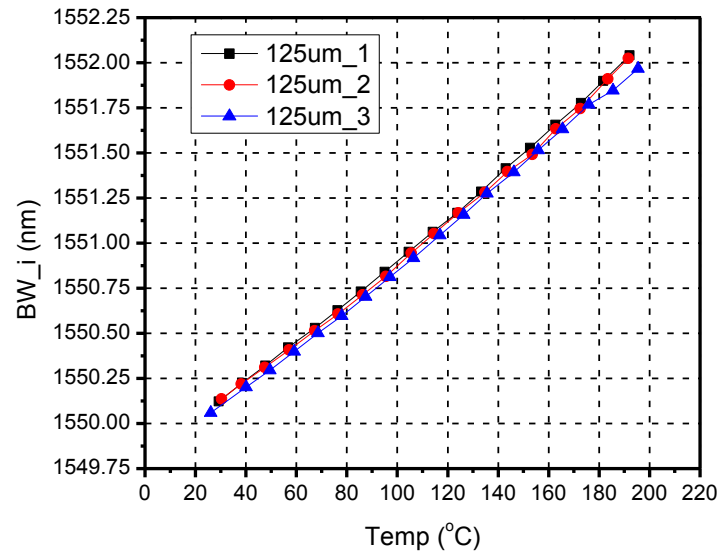
In this section of the study, a newly developed system to accurately measure evolution properties of polymers will be proposed. Proposed system was developed mainly to reduce the problems and challenges mentioned in the previous chapter with improvements. Specific changes or additions made to the existing system will be discussed thoroughly in this chapter.

### **4.1    FBG on Special Fiber**

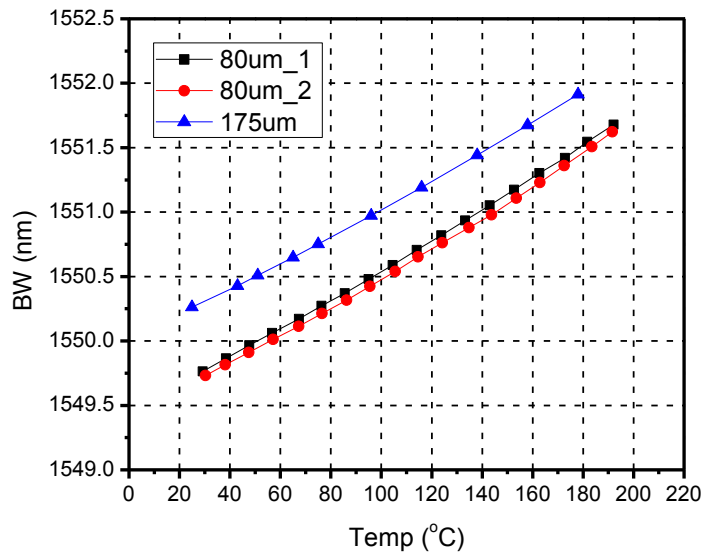
As discussed in previous chapter, heat generation causes major problems which made this application very limited specifically with high exothermic polymers. Heat

generation during polymerization increases the temperature of polymer substrate which makes it difficult to control especially inside the convection oven. There were several ideas that could be implemented to reduce or remove heat generated within polymer substrate during curing. One approach was to reduce insulation around polymer substrate, the silicone rubber tube, and create conduction path for the heat to escape from the polymer substrate and let the temperature equilibrate. However, this was not applicable because it was very difficult to fabricate thin and uniform layer of Silicone that could hold and form perfect shape of cylinder on the metal surface.

Since a certain thickness of soft, low modulus, silicone rubber was to be used to hold polymer in place during curing, the second approach was used to reduce the volume of polymer as much as possible so the amount of heat generated could be minimized. In this proposed system, a unique method is introduced: Special fiber. By using the special fibers with cladding diameter of 80  $\mu\text{m}$  and 175  $\mu\text{m}$ , the polymer substrate diameter did not have to be increased or decreased in order to have a different configuration of specimen. Fabrication or usage of the special fiber for FBG sensors was a new approach. Typically, 125  $\mu\text{m}$  cladding diameter fibers were used for FBG sensor systems. Fabrication of FBG on the special fiber was a challenge, but it was successfully applied. The FBG was fabricated with same procedure on the special 80 $\mu\text{m}$  and 175  $\mu\text{m}$  cladding diameter fibers that have same material and optical properties as the regular, 125 $\mu\text{m}$ , cladding diameter fibers.



(a)



(b)

Figure 11. Intrinsic BW data of FBG's on (a) 125 $\mu\text{m}$  cladding diameter fibers and (b) 80  $\mu\text{m}$  and 175 $\mu\text{m}$  cladding diameter fibers

The Figure 11 shows peak values recorded as temperature changed for 125  $\mu\text{m}$  cladding diameter FBG sensors in (a) and special fibers with 80  $\mu\text{m}$  and 175  $\mu\text{m}$  cladding diameters FBG sensors in (b). The three 125  $\mu\text{m}$  diameter sensors showed very stable and consistent response as temperature changed. FBG on special fibers also showed stable response with slight deviations. Such deviation does not mean that the performance of the FBG on special fiber is poor, but it means that these fibers may have slightly different intrinsic properties from one another.

After successfully fabricating FBG sensors on the special fibers, these were embedded in the polymer substrate to develop combination of different configurations. Previously two configurations shared same dimension of the optical fiber with different diameter of the polymer substrate. In this proposed system, the diameter of the polymer substrate remains constant, but two different optical fibers are used: 175 $\mu\text{m}$  and 80 $\mu\text{m}$  cladding diameter fibers.

System	Fiber Diameter ( $\mu\text{m}$ )	Polymer Diameter (mm)	Configuration ( $\beta$ )
Previous	125	5	40X
	125	2.5	20X
Proposed	175	3.175 (=1/8")	18.14X
	80	3.175 (=1/8")	39.7X

Table 1: Specimen Configurations of the Previous and Proposed Systems

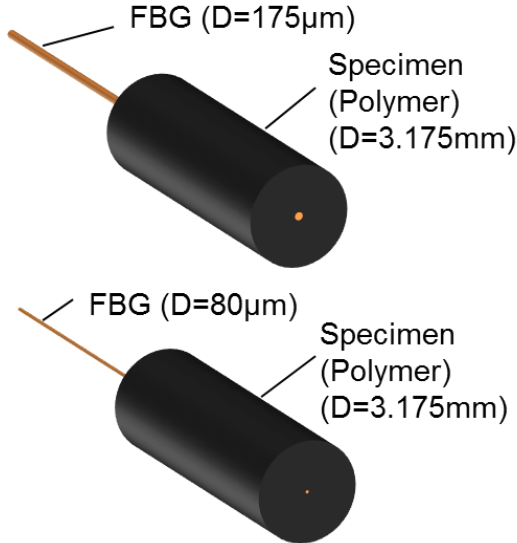


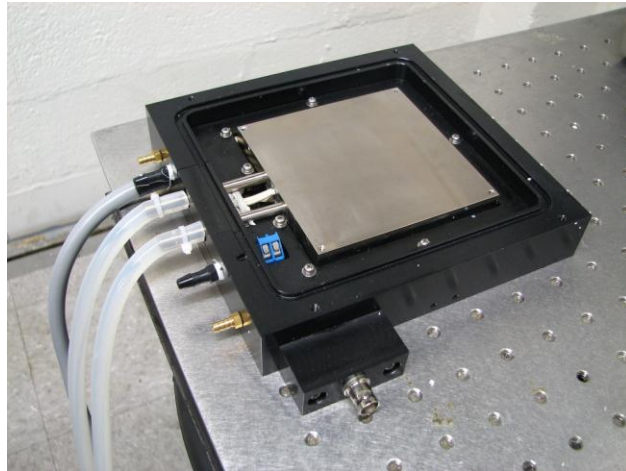
Figure 12. Specimen Configurations with Different Fiber Diameter

The Table 1 shows how two configurations can be obtained with different combinations of fibers and polymer substrate dimensions. The most advantageous reason of using smaller diameter fiber (80 $\mu\text{m}$ ) is that bigger configuration like 40X can be attained with small volume of polymer (3.175mm diameter) which will generate less heat. The heat will still be generated during polymerization however, two configurations will contain same amount of heat being generated since they have the same volume of polymer.

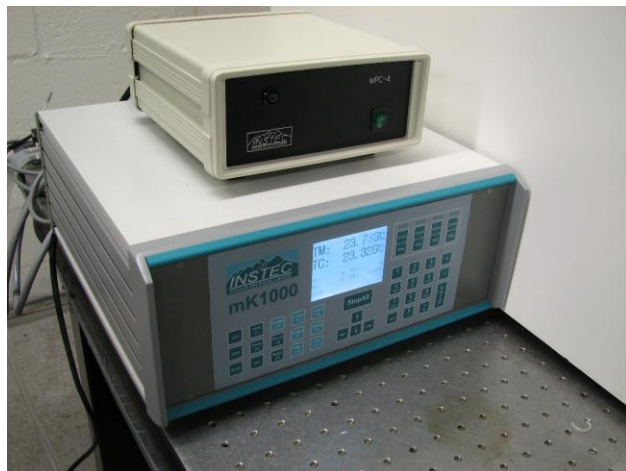
## 4.2 Conduction Heater as Heating Source

In order to effectively control temperature of the system, the convection oven was replaced with conduction heater. Conduction heater can provide higher heating/cooling rate when using highly conductive metal parts, whereas convection oven uses air to heat/cool specimen. A conduction heater and its controller shown in Figure 13 with the

specifications in Table 2 were selected to provide high heating rate, temperature uniformity and precise temperature controllability.



(a)



(b)

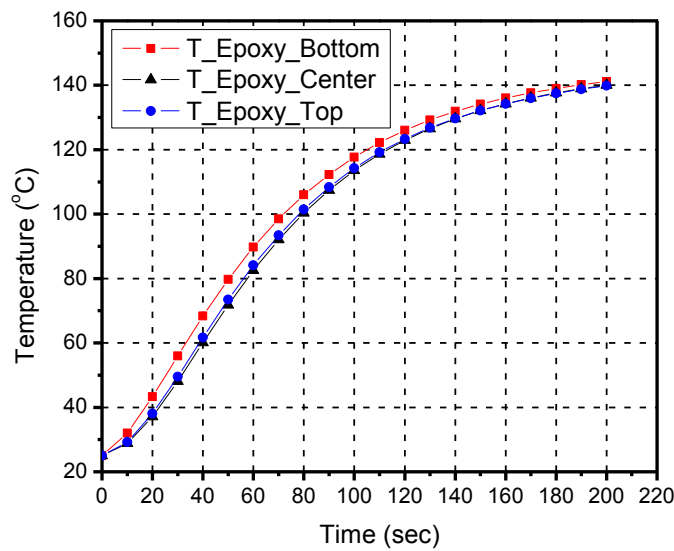
Figure 13. (a) Conduction Heater and (b) Controller

<b>Heating rate</b>	120°C/min
<b>Temperature overshoot</b>	< 0.3°C
<b>Temperature resolution</b>	<0.001°C
<b>High temperature limit</b>	300°C

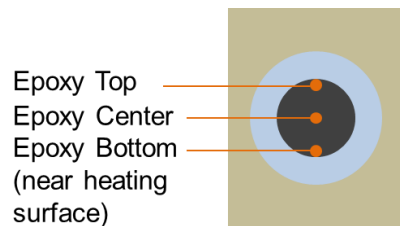
<b>Heating surface area</b>	10cm x 10cm
-----------------------------	-------------

Table 2. Specifications of Conduction Heater

With the specified heater, designed system was modeled and was analyzed to demonstrate its temperature behavior as the results are shown below. The temperature analysis was also used for optimization of the metal mold designs by running the models with different dimensions of the metal molds in order to find the most optimized size and dimensions of the system. Both transient and steady state analysis were conducted using ANSYS Icepak software.



(a)



(b)

Figure 14. (a) Transient Temperature Analysis Result of the Proposed System,  
(b) temperature analysis figure

The transient temperature analysis illustrates three different temperature curves of the temperature at the center of polymer, at the bottom of polymer and at the top of polymer as shown above. During the heating, the temperature gradient is present however, it quickly dies out as it approaches the targeted temperature. Even though the heater has a heating capacity of 120°C/min, when the metal molds were mounted on top of the heating surface, the maximum heating rate dropped to about 60°C due to addition of thermal mass.

Steady-State	
T_Bottom_Mold	147.965
T_Top_Mold	147.466
<b>ΔT_Mold_Top/Bottom</b>	<b>0.499</b>
T_Epoxy_Bottom	147.851
T_Epoxy_Top	147.604
<b>ΔT_Epoxy_Top/Bottom</b>	<b>0.247</b>

Table 3. Steady State Temperature Analysis Result of the Proposed System

The steady state temperature analysis was conducted assuming there is no heat generation within polymer substrate in order to see how the conduction heater and the metal molds will be stabilized at the steady state. The result showed that the maximum temperature gradient within the polymer substrate will be less than 0.3°C and the temperature difference between the center of the bottom mold and at the center of the top mold will be less than 0.5°C which means that the temperature distribution of the entire system will be very uniform with the optimized design and the conduction heating source.

### 4.3 Design Requirements of the Proposed System

Since the main heating source was completely changed from convection oven to conduction heater, the entire design of the system including metal molds had to be changed. Basic concept of the proposed design is illustrated below in Figure 15. Two different size fibers should be embedded inside polymer that cures inside silicone rubber tubes heated within metal molds. In this section, the new design will be proposed with some design challenges and their resolutions.

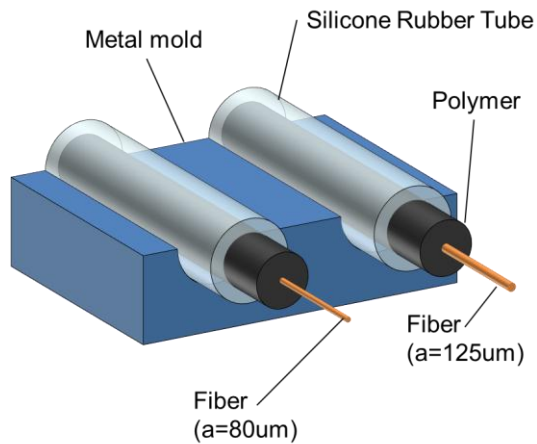


Figure 15. Basic concept of the proposed design

The purpose of the system is to make a system that can (1) form and cure cylindrical shape of polymer with 15mm length, (2) reach temperature stabilization of the specimen as fast as possible with temperature gradient smaller than 1 degree within polymer substrate, (3) align fiber in the center of the polymer substrate without constraining the fiber, and (4) physically not constrain the polymer from expanding or shrinking. The main components of the design include heating surface, heater frame, fiber alignment, metal molds, polymer, and fiber. Since two specimens were to be tested simultaneously, the metal molds had to have two same exact set ups for two specimens.

For fiber alignment, standard V-groove fiber holders were used. These fiber holders are designed to precisely hold and align fibers with magnetic clamps, and were attached to the frame of the heater so the fibers could be aligned and maintained with the system. Metal molds were to be attached to the heating surface directly. The figure below illustrates the basic requirements of this system, and more details were added as the system was designed based on these requirements.

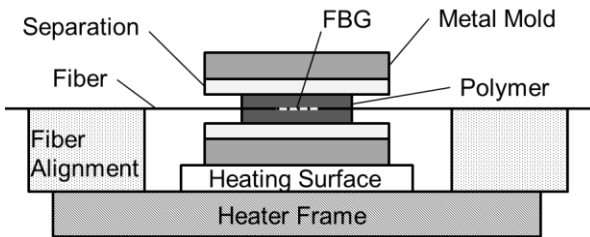


Figure 16. Detailed concept of the proposed design

#### 4.4 Design Specifications of the Proposed System

The metal molds were to be designed to incorporate all the requirements described above, which are repeated below:

- (1) Specimen configuration: Polymer substrate outer diameter of 1/8"
- (2) Temperature stabilization and distribution
- (3) Fiber alignment
- (4) No mechanical constrain on fiber and polymer substrate

An illustration of the proposed design is shown in Figure 17 below.

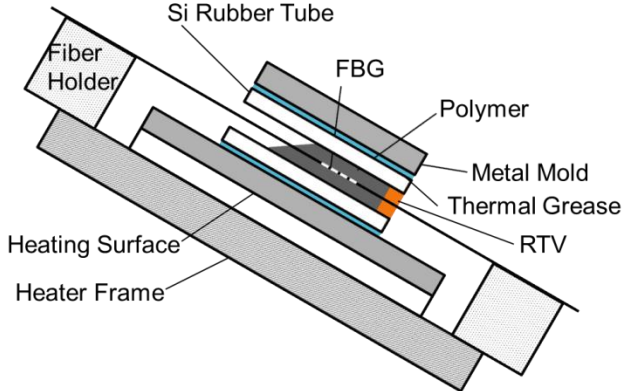
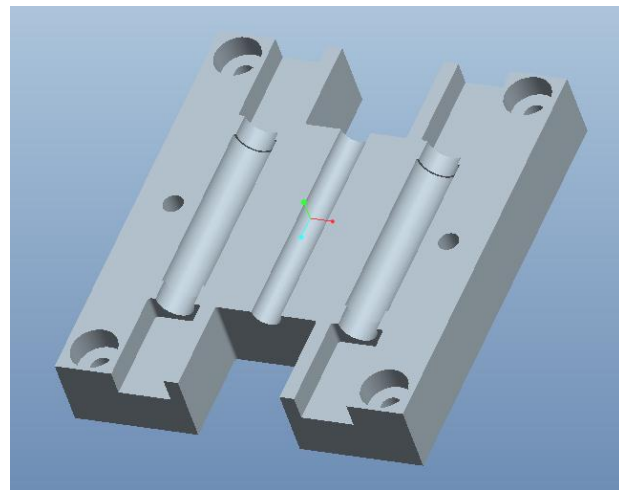


Figure 17. Design illustration of proposed system

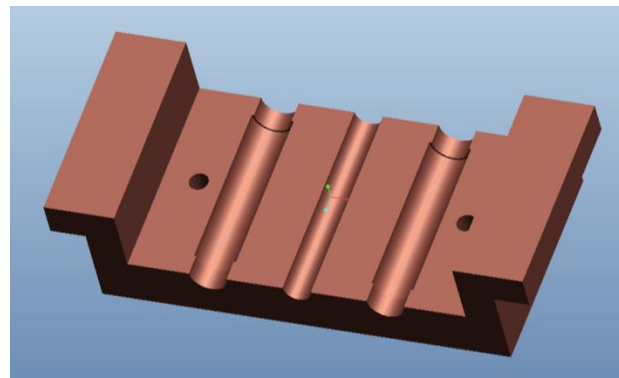
(1) Specimen configuration: In order to fabricate the desired specimen configuration, a silicone rubber tube was used. The inner diameter of the tube is 1/8" and the outer diameter is 1/4 inches, which gives thickness of the tube to be 1/16 inches. Since the uncured polymer is mostly in the state of liquid at working temperature (viscous at room temperature), the tube should be blocked on the end in order to keep the liquid in form. The system was to be rotated at a certain angle and only one end of the tube was required to be blocked. This tube was embedded inside metal molds.

(2) Temperature stabilization and distribution: Since the heating source was changed from convection oven to conduction heater, the molds were designed to meet the temperature requirements. In order to allow fast heat transfer from the heating surface to the specimen, the tube was embedded inside metal molds that were directly sitting on top of the heating surface. Material Aluminum was chosen based on its low material and manufacturing cost and good thermal properties. There was another important aspect of heat transfer within the system: contact resistance. Contact resistance can be reduced by simply using high conductive thermal grease between surfaces in contact. The thermal grease was applied on every surface of physical contacts between the heating surface,

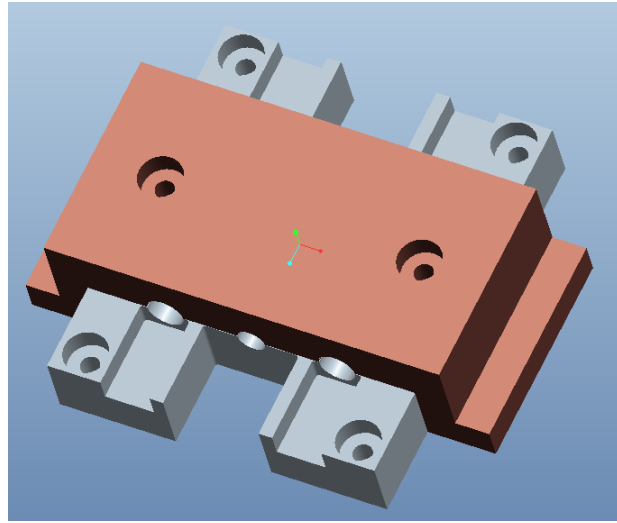
metal molds, silicone rubber tube, etc. The distance between the heating surface and the specimen was kept as low as possible in order to make sure heat is transferred as fast as possible to the specimen. As discussed in the previous chapter, temperature analysis was conducted using ANSYS Icepak software in order to optimize some designs and dimensions of the metal molds. Finalized design of the metal molds that hold the silicone rubber tubes are shown below in Figure 18 (a) - (c).



(a)



(b)

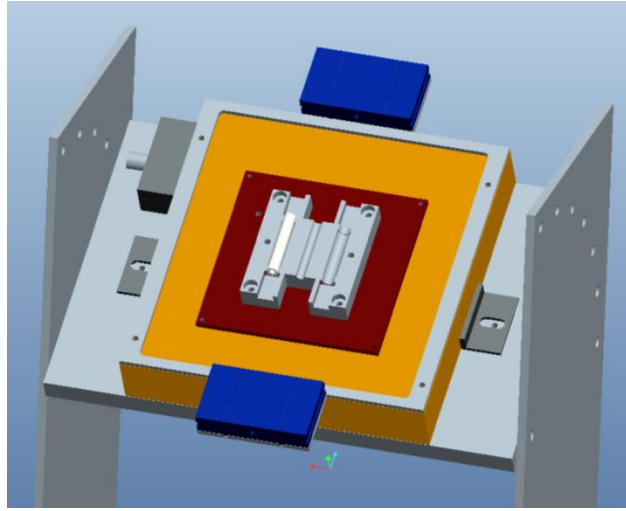


(c)

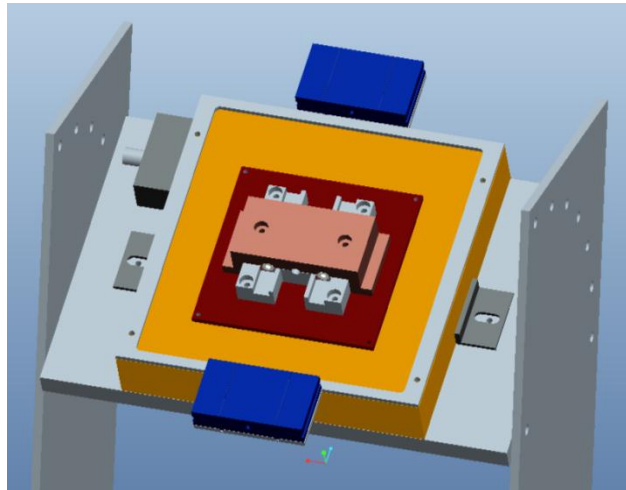
Figure 18. Optimized metal mold designs (a) Bottom mold, (b) Top mold, and (c) Bottom and Top mold assembly

The two channels on the sides are the places where the silicone rubber tubes sit in after thermal grease is applied over all surfaces in contact with another part.

(3) Fiber alignment: It is very important that the fiber is aligned at the center of the polymer substrate as accurate as possible. In order to ensure the location of the fiber, v-groove fiber holders were used. The mold is also designed so that it is aligned with the fiber holders when assembled to the heating surface. When the fiber is fixed on the fiber holder, the fiber should be located at the center of the tube, or the center of the polymer substrate.



(a)



(b)

Figure 19. Fiber alignment system of the proposed system; (a) fiber holders assembled on fiber alignment fixture with bottom mold, and (b) top mold assembled to (a)

As illustrated above in Figure 19, the fiber holders are aligned precisely with the silicone rubber tubes that are inside the metal molds. These v-groove fiber holders are designed to align and hold optical fibers.

(4) Mechanical constrain on fiber and polymer: There should be no constrain on the fiber and the polymer during curing because they both needs to be free from the

environment in order to measure the strain due to chemical shrinkage during curing. The fiber constrain could come from two sources: fiber holder and RTV of the tube on one end.

It is very important that the fiber is not constrained while it is perfectly aligned. In order to make sure the fiber maintains alignment, it should be securely aligned on the fiber holder. However, the magnet clamp or a piece of tape would constrain the fiber and it can affect the BW measurement while shrinkage happens during curing. This was tested in many different ways and the best way to resolve this problem turned out to be to use thick grease to hold the fiber on the fiber holder with a thin piece of tape over it.

As shown in Figure 17, on the side where RTV is cured, the fiber should also not be constrained. A low modulus RTV was selected and a small amount, about 0.1" thick, was cured to block one end of the tube. This RTV had modulus that was low enough not to constrain fiber. However, it was very important that when blocking the bottom end, whatever it was that was used to block the tube could not exert force or grab fiber for the same reason. The solution was to use a low modulus RTV to block the bottom end.

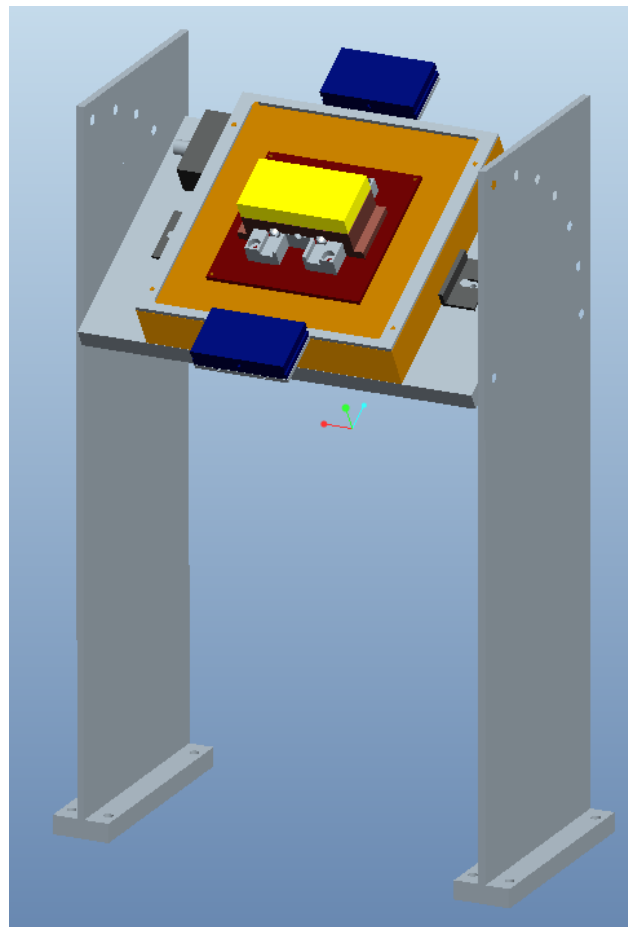
After one end of fiber was aligned with cured RTV and the other end was aligned and fixed with grease and tape, a simple temperature test was conducted to with the FBG sensor in order to examine the presence of constrain on the fiber. As shown below, the fiber was held at the top with grease and tape on the fiber holder, and the other end was aligned and fixed with low modulus RTV. The system was first heated to a high temperature. At high temperature the fiber was pulled from the top in order to ensure it is maintained straight. After pulled, the BW value went back down to its intrinsic BW value at that particular temperature. Then the system was cooled down to room

temperature in order to see whether the fiber can shrink as much as it wants to, due to CTE of the fiber, even when it is fixed at one end with grease and tape and the other end with the low modulus RTV. As shown below, the BW value of the fiber followed its intrinsic property and therefore proved that the grease and tape, and the RTV do not constrain the fiber.

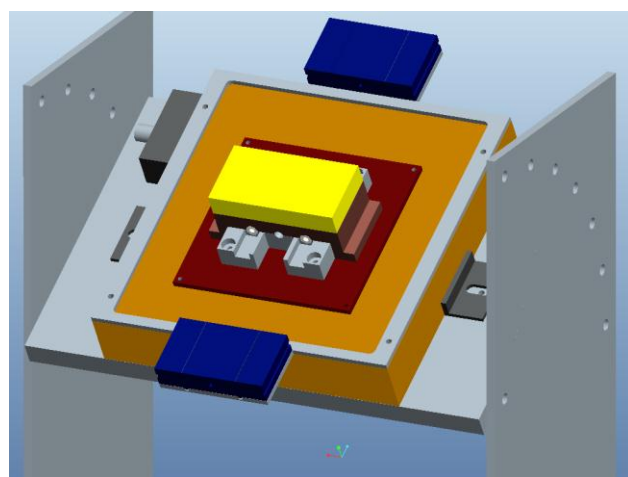
It is also critical to remove or minimize the source of constrain on the polymer substrate itself, because as the polymer cures, it should be free to shrink in order to accurately measure its total chemical shrinkage during curing. The silicone rubber tube acted as a release/separating agent between the polymer and the metal surfaces. It is a well-known fact that the polymer does not adhere to the silicone rubber surface during and after curing. This particular silicone rubber tube was also used in Wang's approach and was proven that the polymer does not get constrained by this tube with its thickness. Thickness of the tube was also important. If too thin, the shrinkage of polymer was constrained. If too thick, the release agent layer acted like a heat insulator and was not helpful for this system.

Another important issue was bubble within the specimen. Underfill material is usually very viscous at room temperature. During injection it is very easy to introduce bubble inside the tube. Since the dimension of the specimen was already small, even a tiny bubble could have been a bigger problem, especially when it ends up forming near the grating area. In order to minimize air bubble inside the specimen, the polymer was to be pre-heated at around 50°C before the injection, as well as the entire system. This way, bubble formation was minimized and therefore reduced errors during property

measurement. With all the design specifications mentioned above, the final design was developed as shown below.



(a)



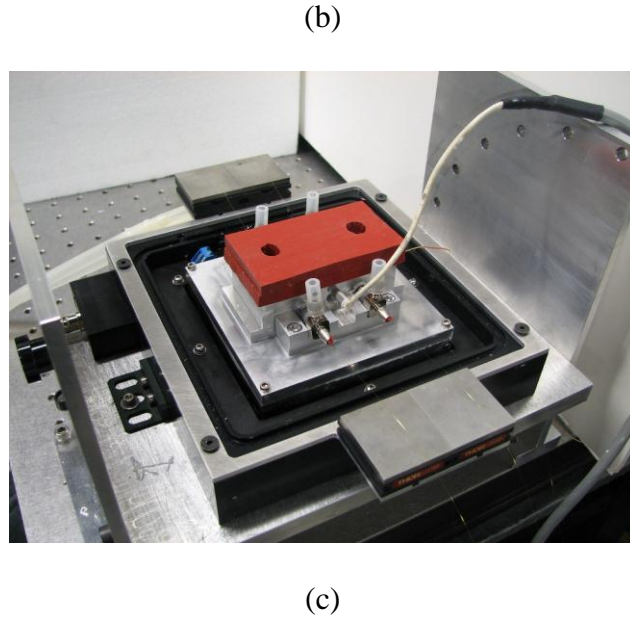


Figure 20. Final proposed design; (a) Machine design of overall structure, (b) Machine design close-up, and (c) Machined parts assembled

Figure 20 (a) represents the machine drawing of overall structure that was designed for the proposed system. In Figure 20 (b), it shows the entire system with everything assembled. A thick insulation rubber layer was adhered to the top surface of the top metal mold that was also optimized in thermal analysis to decrease temperature distribution through thickness or to enhance temperature uniformity. The Figure 20 (c) illustrates the actual designed system where everything is assembled in place. The RTD sensor is embedded on the top mold in order to monitor the temperature of the top mold.

## **Chapter 5. Implementation/ Experiment Procedure**

In this chapter, the experimental and analysis procedures of measuring curing evolution properties will be explained with details.

(1) As discussed in the previous chapter, the specimen was fabricated using metal molds and conduction heater. The metal molds were assembled using thermal grease on surfaces that are in contact with other parts as shown below in Figure 21. The molds include two sets of channels for two specimens, C-1 and C-2, when assembled together. Two pieces of the silicone rubber tube (inner diameter of the tube is  $1/8''$  and outer diameter is  $1/4''$ ) were cut to given size then were inserted inside the metal mold. Thermal grease was also applied between the outer surface of the tubes and the metal molds.

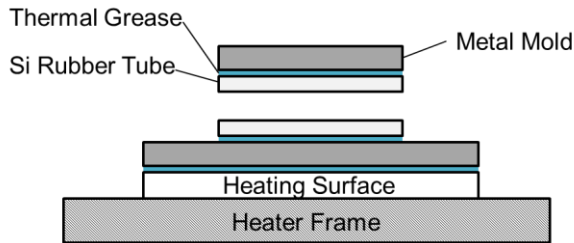


Figure 21. Assembled metal molds and silicone rubber tube

(2) After everything was assembled, the fibers were aligned with RTV as shown below in Figure 22. The RTV was cured at high temperature, because it cures faster, then the heater was set to a temperature of  $50^{\circ}\text{C}$ . The polymer was also preheated at the same temperature before the injection. The fibers were securely aligned and fixed at the fiber holder using grease and tape as described before.

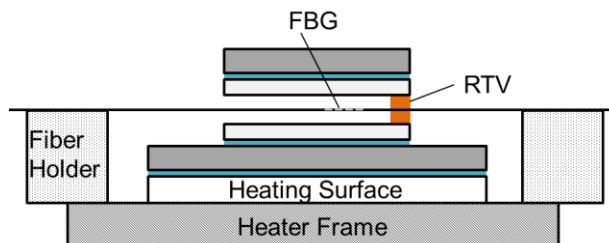


Figure 22. Fiber alignment using RTV

(3) As shown in Figure 23, the system was tilted about 30° because only one end of the tube was blocked with RTV. After everything was pre-heated at 50°C, the polymer was injected from the bottom, where the RTV was cured. Pre-heated polymer was injected using a syringe very slowly to make sure no air bubble is introduced within the specimen in both tubes.

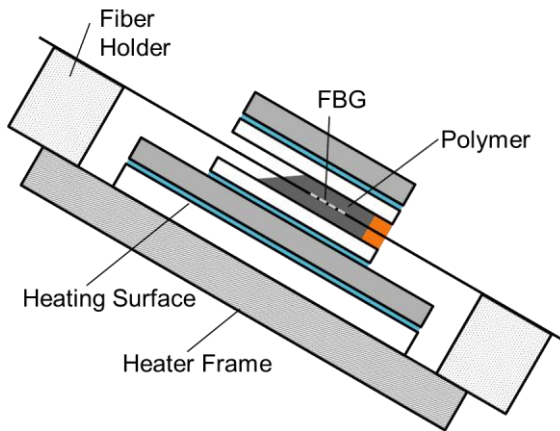


Figure 23. Injection of polymer in tilted system

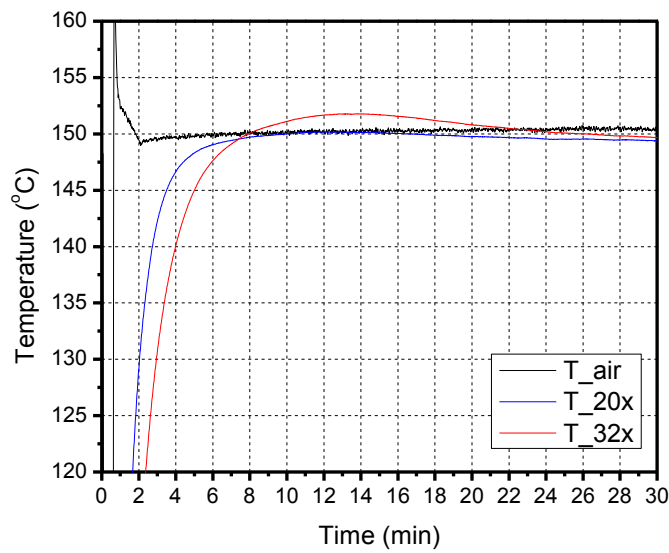
(4) After the preheated polymer was injected in the tubes so the specimen length was 15mm, the system was heated to the curing temperature of polymer. The BW data was recorded starting this point.

(5) After the temperature seemed to be stabilized, i.e. the BW peak data seemed to flatten out, the fiber was pulled with hand from the opposite end of RTV to ensure fiber alignment. After the temperature stabilized, as chemical shrinkage starts to occur, the BW peak data began to drop. As the curing proceeds, the BW will continue to drop until the curing has finished. When BW shows no more decrease than about 10pm for 5 minutes, it can be considered that the curing has completed and the measuring can be stopped.

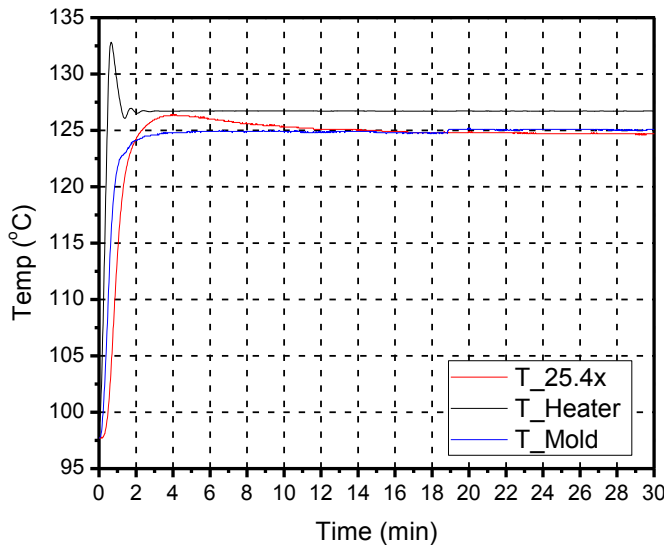
## Chapter 6. Results and Discussion

### 6.1 Temperature Profile of the Proposed System

After the proposed method was implemented, temperature of uncured polymer was monitored and documented during the polymerization in order to understand the temperature profile of the polymer substrate and to compare to the previous method that uses the convection oven. The results are shown below in Figure 24.



(a)



(b)

Figure 24. Temperature profile of polymer during polymerization in (a) Convection oven and (b) Conduction heater

As uncured polymer was injected inside the silicone rubber tubes, thermocouple was embedded in the center of polymer in order to accurately measure the temperature data of polymer substrate in each case. The temperature data for both cases in Figure 24 (a) and (b) are summarized in the Table 4 below.

Heating Source	Specimen Configuration	Overshoot	Stabilization time after peak
Convection Oven	20x	1°C	25min
	32x	3°C	25min
Conduction Heater	25.4x	1.6°C	8min

Table 4. Summary of temperature profile comparison in Figure 24

Underfill material was tested using two different heating sources in order to see how temperature response is different from each other. In the case where the convection

oven was used, the uncured polymer was placed inside the silicone rubber tube and was heated to its curing temperature as the temperature of the polymer and the air inside the oven were recorded. Two specimens were tested in this case: 20x and 32x. 20x specimen showed about 1°C of overshoot and the 32x specimen showed about 3°C of overshoot after heated. After reaching its peak, the temperature stabilized very slowly and reached equilibrium about 25 minutes after the temperature has reached its peak.

In case of the proposed method, where conduction heater and the optimized metal molds were used, specimen size of 25.4x was used, which is approximately in the middle of the 20x and 32x specimen configurations. The 25.4x specimen showed about 1.6°C of overshoot, which is also in between the values of temperature overshoot of 20x and 32x cases. After the temperature reached its peak value, it stabilized much faster than the case of convection. It only took about 8 minutes for the temperature of the polymer to stabilize inside the metal mold, which is a significant progress. Decreasing volume of polymer substrate will decrease the amount of temperature overshoot, and using the conduction heater as heating source will provide much faster heating rate as well as temperature stabilization. This can effectively eliminate problems associated with heat generation of polymer during polymerization.

## 6.2 BW Data for Two Configurations

After the proposed method was implemented, the BW data for both configurations was obtained during polymerization. The plot below contains two 25.4x configurations with lengths 30mm and 15mm.

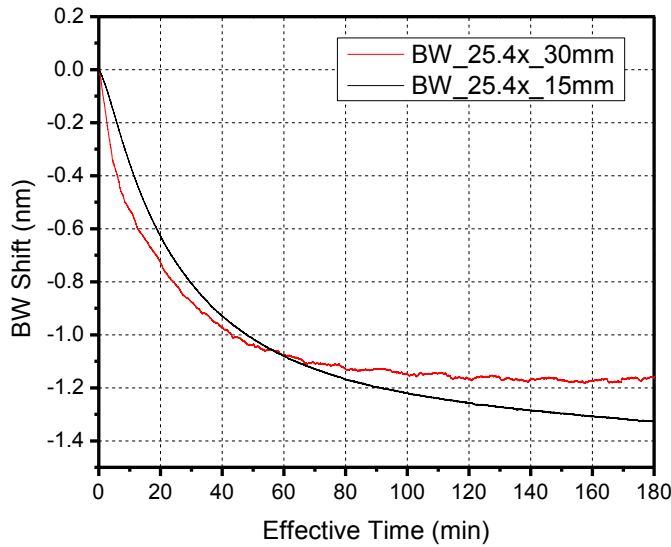
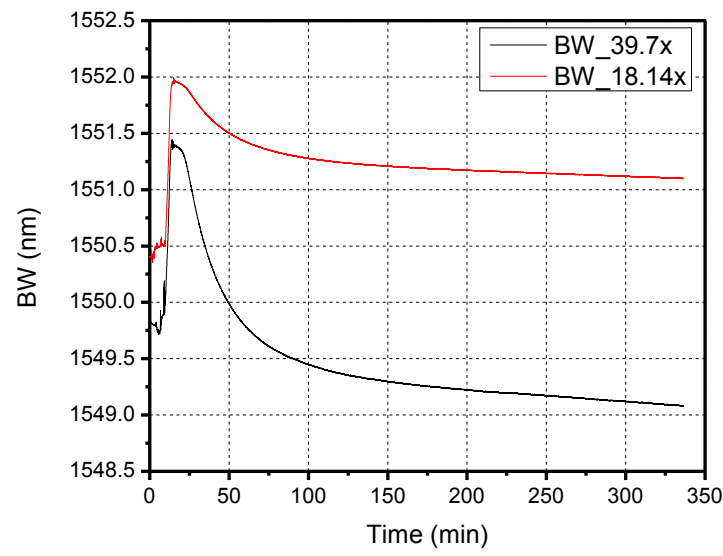
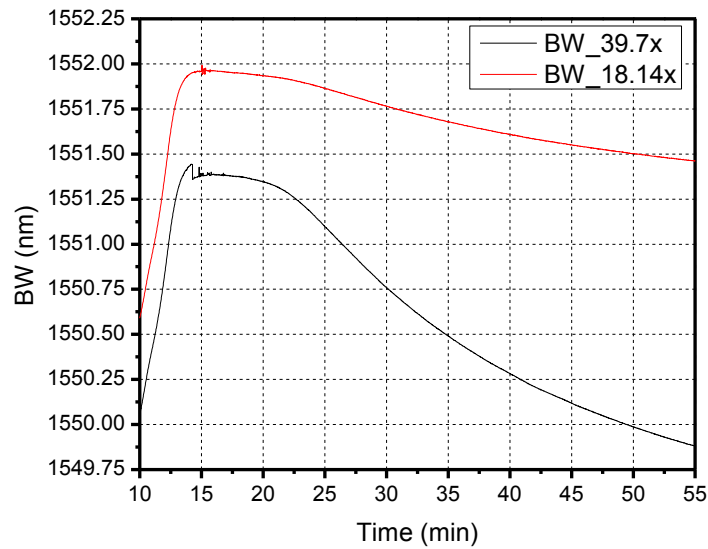


Figure 25. BW Shift data of 25.4x UF-2 specimens with 30mm and 15mm lengths. This plot clearly shows improvement that has been implemented after the length was shortened to 15mm, which is 3 times longer than that of the length of Bragg grating (5mm). The BW shift data of shorter length specimen shows smooth trend as oppose to the specimen of 30mm length. Since 15mm length specimen has much less friction effect than that of 30mm length specimen, there was almost no physical constrain that could possibly come from the friction force on the outer surface of the polymer.

Proposed system was implemented using underfill material UF-2 with special fibers of diameter 80  $\mu\text{m}$  and 175  $\mu\text{m}$ . The raw BW data of the two configurations are plotted.



(a)



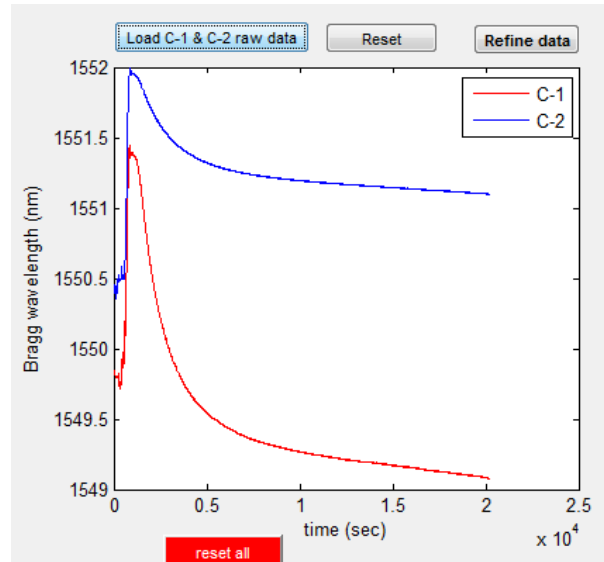
(b)

Figure 26. (a) Raw BW data of two UF-2 specimens recorded during polymerization (b) First 55 minutes after heating started

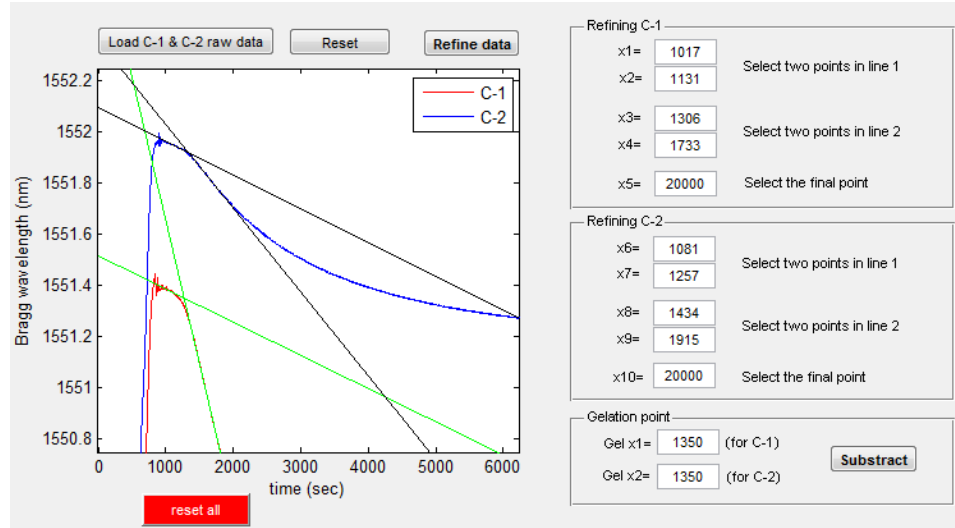
The Figure 26 (a) shows the entire raw BW data for both configurations. In Figure 26 (b), the temperature reached the curing temperature of 175°C within 5 minutes after heating started, and stabilized quickly. (The heating started when  $t=10\text{min}$ ). Some peaks and disturbance of BW shown at  $t=15\text{min}$  are signs of pulling fiber manually for alignment purpose as described in the previous chapter. Ignoring these peaks, it can be observed that the temperature control of this system successfully stabilized the temperature of the specimen before the apparent gelation point.

### 6.3 Gelation Point Determination and Deformed BW Data

After the raw data was obtained, it can be analyzed to calculate effective chemical shrinkage and modulus evolution during curing using the software MATLAB. Data for both configurations, C-1 and C-2, are loaded in the MATLAB program and plotted as shown below in Figure 27.



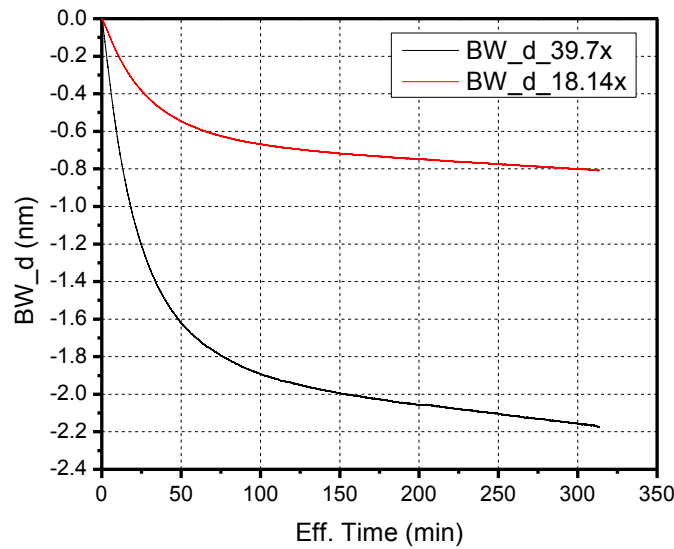
(a)



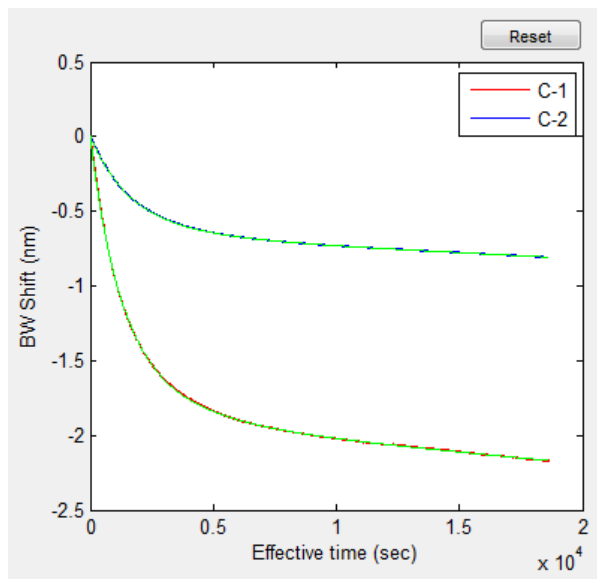
(b)

Figure 27. (a) Raw BW data loaded for both configurations C-1 and C-2, (b) Determination of gelation point for both configurations

Gelation point for both BW data is determined as the inflection point, or the interception of the two lines, one plateau area and one after BW starts to drop. After gelation point is determined, the data is re-plotted in order to show the deformed BW data, or the BW shift data, by subtracting the BW value at the plateau area. The BW shift data will only show BW change due to deformation of FBG induced by curing polymer. After the data is formatted, the formatted data for both configurations will be plotted as shown below in Figure 28. The formatted data is then smoothed and fitted to a functional form for the next step.



(a)

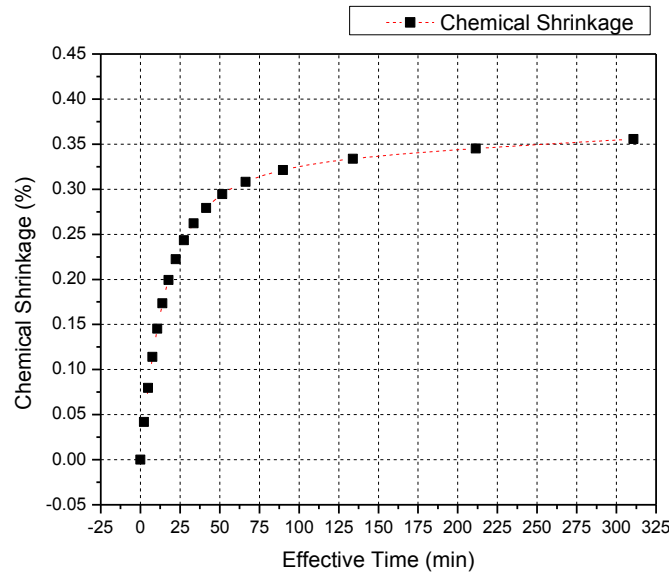


(b)

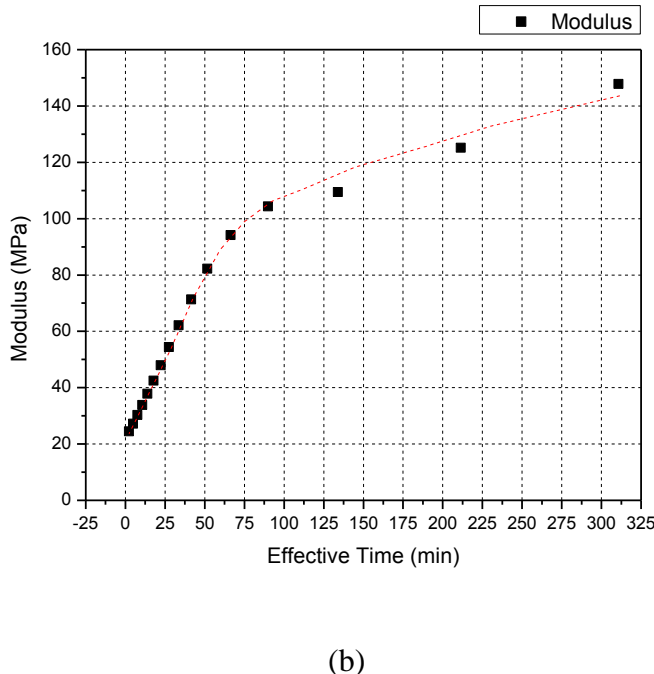
Figure 28. (a) Deformed BW data of both configurations, C-1 (125um FBG) and C-2 (80um FBG), (b) Fitted data

## 6.4 Step Size Input and Calculations of Effective Chemical Shrinkage and Modulus Evolutions

After the raw data has been formatted to deformed BW data as shown above in Figure 28, the data is then analyzed to calculate curing evolution properties of polymer. First the raw data is fitted in MATLAB using the curve fitting toolbox. After fitted, the data is analyzed following Wang's procedure where they are first divided with a constant "BW step-size". This number is defined by the user, depending on how many number of points the user wants to see in the calculation. In this case, step size of 10pm was selected and the calculation results are shown below.



(a)



(b)

Figure 29. Evolution properties of UF-2 (1) effective chemical shrinkage, and (2) modulus

The results show that the effective chemical shrinkage of UF-2 material evolves to the value of about 0.36% and the modulus of the polymer evolves to the value of about 148MPa during the polymerization.

## Chapter 7. Conclusions

An advanced measurement technique based on fiber Bragg grating (FBG) sensor was proposed to measure critical properties of polymeric material during polymerization: effective chemical shrinkage and modulus evolutions. The existing technique proposed by Yong Wang, University of Maryland, that established this method was closely investigated especially in the implementation stage then modifications and improvements

were made to overcome the challenges and difficulties associated with the existing system.

The proposed method enhances the measurement by reducing exothermic heat generated during polymerization and improving temperature stabilization which can lead to clear determination of gelation point of both specimens cured simultaneously. In order to reduce exothermic heat being generated during polymerization special fibers were used to fabricate Fiber Bragg Grating. Using these special fibers two configurations were created using same polymer dimension. Temperature stabilization was enhanced by changing heating source from convection chamber to conduction heater, which provided high heating rate and precise temperature stabilization. The newly designed system was optimized based on changes made in order to ensure fiber alignment, temperature stabilization and distribution, and no mechanical constrain applied to the specimen during measurement. The proposed method was implemented using an underfill material which had 0.36% total effective chemical shrinkage and evolution of modulus to final value of 148MPa.

This technique can now be used to measure critical properties of polymers with high polymerization exothermic heat. It can also be used further to characterize other material properties of polymeric materials such as CTE and viscoelastic properties. This way this technique can potentially provide all material properties of interest to packaging engineers including Coefficient of Thermal Expansion and viscoelastic properties with just two specimens.

This technique can also be implemented in industry where characterization of polymeric materials is highly desired. The proposed technique is optimized and designed to be routinely performed by technicians while fulfilling the purpose of this technique.

# Appendix

## A. Analytical solution of the stress fields within the FBG [12]

The fiber is assumed to be a solid cylinder with outer radius  $a$ , while the substrate has inner radius  $a$  and outer radius  $b$ . The subscripts, “ $f$ ” and “ $s$ ” are used to identify the fiber and substrate parameters, respectively. The general elastic solution can be expressed as:

$$\sigma_{rr}(r) = -\frac{\alpha_f E_f}{1-\nu_f} \frac{1}{r^2} \int_0^r r T(r) dr + \frac{E_f}{1+\nu_f} \left[ \frac{C_{1f}}{1-2\nu_f} - \frac{C_{2f}}{r^2} \right], \quad 0 \leq r \leq a, \quad (\text{A-1})$$

$$\sigma_{\theta\theta}(r) = \frac{\alpha_f E_f}{1-\nu_f} \left[ \frac{1}{r^2} \int_0^r r T(r) dr - T(r) \right] + \frac{E_f}{1+\nu_f} \left[ \frac{C_{1f}}{1-2\nu_f} + \frac{C_{2f}}{r^2} \right], \quad 0 \leq r < a \quad (\text{A-2})$$

$$\sigma_{rr}(r) = -\frac{\alpha_s E_s}{1-\nu_s} \frac{1}{r^2} \int_a^r r T(r) dr + \frac{E_s}{1+\nu_s} \left[ \frac{C_{1s}}{1-2\nu_s} - \frac{C_{2s}}{r^2} \right], \quad a \leq r \leq b, \quad (\text{A-3})$$

$$\sigma_{\theta\theta}(r) = \frac{\alpha_s E_s}{1-\nu_s} \left[ \frac{1}{r^2} \int_a^r r T(r) dr - T(r) \right] + \frac{E_s}{1+\nu_s} \left[ \frac{C_{1s}}{1-2\nu_s} + \frac{C_{2s}}{r^2} \right], \quad a < r \leq b \quad (\text{A-4})$$

$$\sigma_{zz}(r) = \left[ \nu(\sigma_{rr} + \sigma_{\theta\theta}) - E\alpha T(r) \right] + \sigma_{zz}^0. \quad (\text{A-5})$$

In the loading condition of the piecewise constant temperature distribution,

$$T(r) = \begin{cases} T_f, & 0 \leq r < a \\ T_s, & a < r \leq b \end{cases} \quad (\text{A-6})$$

The general solution given from (A-1) to (A-4) are reduced to

$$\sigma_{rr}(r) = -\frac{\alpha_f E_f T_f}{2(1-\nu_f)} + \frac{E_f}{1+\nu_f} \left[ \frac{C_{1f}}{1-2\nu_f} - \frac{C_{2f}}{r^2} \right], \quad 0 \leq r \leq a, \quad (\text{A-1'})$$

$$\sigma_{\theta\theta}(r) = -\frac{\alpha_f E_f T_f}{2(1-\nu_f)} + \frac{E_f}{1+\nu_f} \left[ \frac{C_{1f}}{1-2\nu_f} + \frac{C_{2f}}{r^2} \right], \quad 0 \leq r < a \quad (\text{A-2'})$$

$$\sigma_{rr}(r) = -\frac{\alpha_s E_s T_s}{1-\nu_s} \frac{r^2 - a^2}{2r^2} + \frac{E_s}{1+\nu_s} \left[ \frac{C_{1s}}{1-2\nu_s} - \frac{C_{2s}}{r^2} \right], \quad a \leq r \leq b, \quad (\text{A-3'})$$

$$\sigma_{\theta\theta}(r) = -\frac{\alpha_s E_s T_s}{1-\nu_s} \frac{r^2 + a^2}{2r^2} + \frac{E_s}{1+\nu_s} \left[ \frac{C_{1s}}{1-2\nu_s} + \frac{C_{2s}}{r^2} \right], \quad a < r \leq b \quad (\text{A-4'})$$

The coefficients can be expressed as

$$C_{1s} = \frac{A+B}{C+D}$$

$$C_{2s} = C_{1s} \frac{b^2}{1-2\nu_s} - \frac{1+\nu_s}{1-\nu_s} \frac{\alpha_s T_s}{2} (b^2 - a^2)$$

$$\begin{aligned} C_{1f} &= C_{1s} \left( 1 - \frac{b^2}{a^2} \right) \frac{E_s}{E_f} \frac{(1+\nu_f)(1-2\nu_f)}{(1+\nu_s)(1-2\nu_s)} \\ &+ \frac{(1+\nu_f)(1-2\nu_f)}{1-\nu_f} \frac{\alpha_f T_f}{2} + \frac{E_s}{E_f} \left( \frac{b^2}{a^2} - 1 \right) \frac{(1+\nu_f)(1-2\nu_f)}{1-\nu_s} \frac{\alpha_s T_s}{2} \end{aligned}$$

$$C_{2f} = 0$$

where

$$A = \left( \frac{b^2}{a^2} - 1 \right) \frac{\alpha_s T_s}{1-\nu_s} \left[ \frac{1+\nu_s}{2} - \frac{(\nu_f - \nu_s) \frac{E_s}{E_f}}{1 + \frac{E_s}{E_f} \left( \frac{b^2}{a^2} - 1 \right)} \right] + \frac{\alpha_f T_f}{1-\nu_f} \left[ \frac{1+\nu_f}{2} - \frac{(\nu_f - \nu_s)}{1 + \frac{E_s}{E_f} \left( \frac{b^2}{a^2} - 1 \right)} \right]$$

$$B = \left\{ \frac{E_s}{E_f} \left( \frac{b^2}{a^2} - 1 \right) \frac{\alpha_s T_s}{2} \frac{(1 + \nu_f)(1 - 2\nu_f)}{(1 - \nu_s)} + \frac{\alpha_f T_f}{2} \frac{(1 + \nu_f)(1 - 2\nu_f)}{(1 - \nu_f)} \right\}$$

$$\times \left\{ 1 + \frac{2\nu_f(\nu_f - \nu_s)}{(1 + \nu_f)(1 - 2\nu_f) \left[ 1 + \frac{E_s}{E_f} \left( \frac{b^2}{a^2} - 1 \right) \right]} \right\}$$

$$C = I + \frac{b^2}{a^2} \frac{1}{1 - 2\nu_s} - \frac{E_s}{E_f} \frac{2\nu_s(\nu_f - \nu_s) \left( \frac{b^2}{a^2} - 1 \right)}{(1 + \nu_s)(1 - 2\nu_s) \left[ I + \frac{E_s}{E_f} \left( \frac{b^2}{a^2} - 1 \right) \right]}$$

$$D = \frac{E_s}{E_f} \left( \frac{b^2}{a^2} - 1 \right) \frac{(1 + \nu_f)(1 - 2\nu_f)}{(1 + \nu_s)(1 - 2\nu_s)} \left\{ I + \frac{2\nu_f(\nu_f - \nu_s)}{(1 + \nu_f)(1 - 2\nu_f) \left[ I + \frac{E_s}{E_f} \left( \frac{b^2}{a^2} - 1 \right) \right]} \right\}$$

## References

1. Chung, D., *Materials for electronic packaging*. 1995: Butterworth-Heinemann.
2. Menges, T.A.O.a.G., *MAterials science of poymers for engineers*. 2003, Cincinnati: Hanser Gardner Publications, Inc.
3. Rodriguez, F., *Principles of polymer systems*. 1996, Washington DC: Taylor & Francis Inc.
4. Gillespie, T.A.B.a.J.W., *Process-induced stress and deformation in thick-section thermoset composite laminates*. Journal of Composite Materials, 1992. **26**: p. 626-669.
5. F. Su, L.L., and T. Wang, *Evaluation of residual stress in flip chip using 3-D optical Interferometry/FEM hybrid technique*. Strain, 2007. **43**: p. 289-298.
6. M. Y. Tsai, C.H.J.H., and C. T. O. Wang, *Investigation of thermomechanical behaviors of flip chip BGA packages during manufacturing process and thermal cycling*. Ieee Transactions on Components and Packaging Technologies, 2004. **27**: p. 568-576.
7. W. G. Zhang, D.W., B. Z. Su, S. A. Hareb, Y. C. Lee, and B. P. Masterson, *The effect of underfill epoxy on warpage in flip-chip assemblies*. Ieee Transactions on Components Packaging and Manufacturing Technology Part A, 1998. **21**: p. 323 - 329.
8. Wong, D.L.a.C.P., *Materials for Advanced Packaging*. 2009: Springer-Verlag New York Inc.
9. J. Lange, S.T., J. A. E. Manson, and A. Hult, *Residual stress build-up in thermoset films cured above their ultimate glass transition temperature*. Polymer, 1995. **35**: p. 3135-3141.
10. A. B. Spoelstra, G.W.M.P., and H. E. H. Meijer, *Chemorheology of a highly filled epoxy compound*. Polymer Engineering and Science, 1996. **36**: p. 2153-2162.
11. S. A. Newman, G.F., B. Hinner, C. W. Maier, and E. Sackmann, *Phase transformations in a model mesenchymal tissue*. Physical Biology, 2004. **1**: p. 100-109.
12. Wang, Y., *Integrated Measurement Technique To Measure Curing Process-dependent Mechanical And Thermal Properties Of Polymeric Materials Using Fiber Bragg Grating Sensors*, in *Mechanical Engineering*. 2009, University of Maryland: College Park.
13. W. W. Morey, C.W.M., and W. H. Clenn, *Fiber optic Bragg grating sensors*. Proceeding SPIE, Fiber Optics and Laser Sensors VII, 1989. **1169**: p. 10.
14. Meltz, K.O.H.a.G., *Fiber Bragg grating technology fundamentals and overview*. Journal of Lightwave Technology, 1997. **15**: p. 1263-1276.
15. A. D. Kersey, M.A.D., H. J. Patrick, M. LeBlanc, K. P. Koo, C. G. Askins, M. A. Putnam, and E. J. Friebel, *Fiber grating sensors*. Journal of Lightwave Technology, 1997. **15**: p. 1442-1463.
16. El-Sherif, R.G.a.M.A., *Analysis of induced-birefringence effects on fiber Bragg gratings*. Optical Fiber Technology, 2000. **6**: p. 299-323.

17. Y. Eom, L.B., V. Michaud, P. Sunderland, and J. A. Manson, *Time-cure-temperature superposition for the prediction of instantaneous viscoelastic properties during cure*. Polymer Engineering and Science, 2000. **40**: p. 1281-1292.
18. McGee, S.H., *CURING CHARACTERISTICS OF PARTICULATE-FILLED THERMOSETS*. Polymer Engineering and Science, 1982. **22**: p. 484-491.
19. P. K. Maji, A.K.B., *Influence of Number of Functional Groups of Hyperbranched Polyol on Cure Kinetics and Physical Properties of Polyurethanes*. Journal of Polymer Science Part a-Polymer Chemistry, 2009. **47**: p. 731-745.
20. Z. H. Luo, L.H.W., W. W. Li, F. Liu, and T. Zhao, *Isothermal differential scanning calorimetry study of the cure kinetics of a novel aromatic maleimide with an acetylene terminal*. Journal of Applied Polymer Science, 2008. **109**: p. 525-529.
21. Wong, Z.Q.Z.a.C.P., *Modeling of the curing kinetics of no-flow underfill in flip-chip applications*. Ieee Transactions on Components and Packaging Technologies, 2004. **27**: p. 383-390.
22. W. W. Li, F.L., L. H. Wei, and T. Zhao, *Curing behavior study of polydimethylsiloxane-modified allylated novolac/4,4'-bismaleimidodiphenylmethane resin*. Journal of Applied Polymer Science, 2008. **107**: p. 554-561.
23. L. Gonzalez, X.R., J. M. Salla, A. Mantecon, and A. Serra, *Kinetic analysis by DSC of the cationic curing of mixtures of DGEBA and 6,6-dimethyl (4,8-dioxaspiro[2.5]octane-5,7-dione)*. Thermochimica Acta, 2007. **464**: p. 35-41.
24. Wang, Y., B. Han, D.W. Kim, *Simultaneous Measurement of Effective Chemical Shrinkage and Modulus Evolutions During Polymerization*. Experimental Mechanics, 2011. **51**: p. 1155-1169.